

A Quantum Klystron - Controlling Quantum Systems with Modulated Electron Beams

Dennis Rätzel,^{1,*} Daniel Hartley,² Osip Schwartz,³ and Philipp Haslinger^{2,†}

¹*Institut für Physik, Humboldt-Universität zu Berlin, Newtonstrae 15, 12489 Berlin, Germany*

²*Vienna Center for Quantum Science and Technology,*

Atominstytut, TU Wien, Stadionallee 2, 1020 Vienna, Austria

³*Dept. of Physics, University of California, 366 LeConte Hall, MC 7300 Berkeley, USA*

Coherent control of quantum transitions generally relies on interactions of the quantum system with electromagnetic waves. We show that the electromagnetic near-field of a current-modulated free-space electron beam can be employed for coherent manipulation of quantum systems. Using Rabi oscillations between hyperfine levels of potassium atoms and magnetic sublevels in nitrogen vacancy centers as examples, we demonstrate that such manipulation can be performed with only classical control over the electron beam itself, and is readily realizable with current technology. Potential challenges like shot noise and decoherence through back action on the electrons are found to be insignificant for our implementation. These results provide a pathway towards electron-mediated delivery of spatially and spectrally tailored electromagnetic fields for quantum control on the nano-scale.

Coherent manipulation of quantum systems is one of the key elements of quantum enhanced metrology [1, 2] and quantum information processing [3, 4]. Traditionally, electromagnetic (EM) fields, such as laser or microwave pulses, are employed to enable control of quantum systems. For these setups, the spatial resolution is generally determined either by the wavelength of the radiation or the size of the antenna used to enhance the field in a sub-wavelength region [5, 6]. In contrast, the small de Broglie wavelength of electrons, utilized in electron microscopy to great effect [7], allows for selective addressing of quantum systems on the nano-scale [8, 9].

Here, we demonstrate that the EM near field of a current modulated electron beam provides an alternative method of coherent manipulation of quantum systems. This approach is reminiscent of a classic type of microwave (MW) amplifier known as a klystron [10, 11], wherein the electron beams velocity is modulated by a periodic seed field, resulting in a current modulation downstream of the interaction region. The kinetic energy of the modulated electron beam is then converted into electromagnetic excitations in a MW cavity (see Fig.1a). Our proposal can be seen as a quantum counterpart to the klystron, where the kinetic energy of a modulated electron beam is converted into a coherent excitation of a quantum system, as shown in Fig.1b.

Apparent obstacles, such as decoherence due to noise in the driving signal (e.g. shot noise) or entanglement between the electrons and the quantum system (back-action), lead to the following three conditions for feasible implementations of our proposal:

1. the back action on the electrons is small enough such that the decoherence accompanying the interaction of electrons and quantum system can be neglected,
2. the beam modulation (one of its spectral lines) is close to resonance with the quantum transition,
3. all relevant decay rates and decoherence rates are small

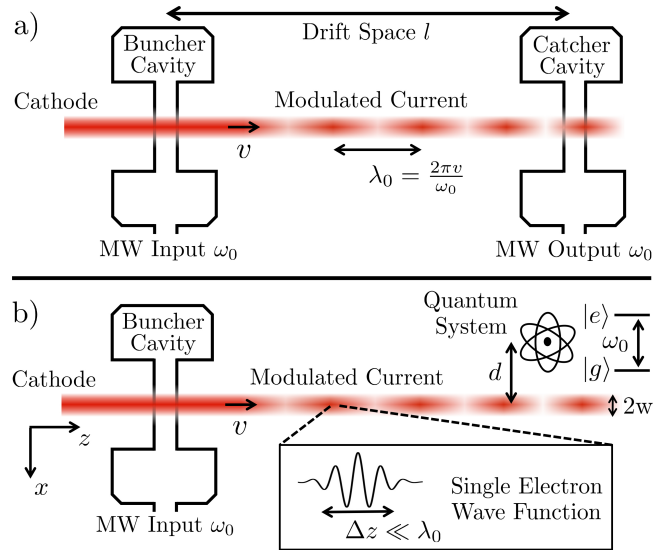


FIG. 1a) Schematic view of a klystron: An electron beam is velocity modulated by the electric field of a microwave (MW) cavity, the "buncher cavity", at frequency ω_0 . Through the drift space, the velocity modulation causes a current modulation, which induces amplified microwaves at the catcher cavity. The amplified MW radiation is used, for example, to drive atomic transitions coherently and with high fidelity. b) Schematic view of our proposed scheme: the electromagnetic near field of the current-modulated electron beam at the position of the catcher cavity is used directly to drive transitions of quantum systems without the detour of generating electromagnetic radiation. w is the electron beam waist, λ_0 is the modulation wavelength, which is much larger than the single electron wave function Δz and d is the distance from the quantum system to the beam center.

in comparison to the inverse of the transition time-scale.

While it has been proposed [12, 13] that quantum systems can coherently interact with a stream of electrons with

spatially tailored wave functions, we theoretically demonstrate that electron-mediated manipulation of quantum systems can be achieved with only classical control over the electron beam, without the need to maintain longitudinal coherence of the electron wave functions.

As a specific implementation, we propose driving magnetic dipole transitions in the MW regime with a modulated electron beam as created, for example, in a classical klystron (see Sec.2 of Supplemental Material (SM) [14]). Since we focus on magnetic dipole transitions, we restrict our considerations to the magnetic dipole interaction $\hat{H}_{\text{int}} = -\hat{\mu} \cdot \hat{B}$, although the general scheme can also be applied to electric dipole or higher multipole transitions. We consider two specific examples: a ground-state hyperfine transition in potassium atoms and a transition between magnetic sublevels in a nitrogen vacancy (NV) center, and show that electron-mediated coherent control is feasible in both systems with existing technology. To this end, we start by discussing Condition 1 in detail.

Back-action – The action of the electrons on a quantum system is accompanied by back action on the electrons [15]. If the change of state of the electrons is in principle detectable, decoherence occurs in the reduced state of the quantum system. We now demonstrate that the back action on the electrons is small enough to allow for coherent driving. We assume that the quantum system is initially in the excited state $|e\rangle$ and consider an interaction with a free electron in the state $|\text{in}\rangle_{\text{el}}$. To the lowest order, after the electron and the quantum system have interacted, the full state will be

$$|\text{out}\rangle = \sqrt{1-P}|e\rangle \otimes |\text{in}\rangle_{\text{el}} + \sqrt{P}|g\rangle \otimes |\text{out}\rangle_{\text{el}}, \quad (1)$$

where P is the transition probability and $|\text{out}\rangle_{\text{el}}$ is the final state of the electron given an accompanying $|e\rangle$ to $|g\rangle$ transition of the quantum system. The driving process can only be coherent if the reduced density matrix $\varrho_a = \text{Tr}_{\text{el}}[|\text{out}\rangle\langle\text{out}|]$ (the partial trace is taken over the electron Hilbert space) is close to a pure state. Therefore, the norm of the overlap of the electron's in-state and its out-state must be close to one.

We assume that the quantum system's dimensions are much smaller than its distance to the center of the electron beam d and the modulation wave length $\lambda_0 = 2\pi v/\omega_0$, where v is the average velocity of the electrons and ω_0 is the radian frequency of the modulation and the transition frequency of the quantum system. Thus, we can consider the quantum system as point-like. Furthermore, for the electron state, we consider an initial Gaussian matter-wave packet of longitudinal size $\Delta z \ll \lambda_0$ such that the beam modulation is not on the level of the single electron wave function but corresponds to correlations between electrons. The transversal width of the Gaussian matter-wave packets is bound from above by the focal width of the beam as $\Delta r_{\perp} < w/2$ and in our specific implementation, we consider $d \sim 5w$. This implies that $d \gg \Delta r_{\perp}$ and the amplitude of the electron

wave function is approximately zero at the position of the quantum system. Furthermore, we restrict our considerations to the case of $d \ll \gamma\lambda_0$, where $\gamma = (1-v^2/c^2)^{-1/2}$ is the Lorentz factor and we neglect the much weaker effect of the electron spin. Under these conditions, the norm of the overlap between the electron in-state and out-state is found to be approximately the overlap of the initial Gaussian wave packet and the same wave packet shifted by the longitudinal momentum transfer $\delta p_z = \hbar\omega_0/v$, which amounts to (see Sec.1 of SM [14])

$$|{}_{\text{el}}\langle\text{in}|\text{out}\rangle_{\text{el}}| \approx e^{-\frac{\Delta z^2 \delta p_z^2}{2\hbar^2}}. \quad (2)$$

We obtain the condition $\delta p_z \ll \hbar/\Delta z$ for the overlap in equation (2) to be close to one, which implies $\Delta z \ll \lambda_0/(4\pi)$. Note that a small size of the electron wave packet is beneficial here. For driving frequencies of up to ~ 10 GHz and velocities of $\sim c/3$ (corresponding to a kinetic energy of $E_{\text{kin}} \sim 30$ keV), we find $\lambda_0/(4\pi) \sim 10^{-3}$ m. The size of electron wave packets Δz is defined by the lifetime of electron states in the source which is limited due to phonon-electron and electron-electron scattering [16, 17]. According to the literature on electron microscopy/interferometry [7, 18], the size of single electron wave packets from the corresponding sources is on the order of $\Delta z \sim 100$ nm. Thus, we conclude that the electron in-state and out-state are nearly indistinguishable and our Condition 1 is fulfilled.

The magnetic field – Electrons from conventional electron sources can be assumed to be uncorrelated [19] and the Pauli exclusion principle does not play a role, which is shown by a degeneracy parameter much smaller than one [18, 20]. Due to these reasons, since $\Delta z \ll \lambda_0$ and Condition 1 is fulfilled, we can model the beam as an ensemble of classical point-like charged particles. For an electron moving with a velocity v parallel to the z -axis with a displacement of $\vec{r}_{\perp} = (x, y)$, whose trajectory pierces the $z = 0$ plane at time t_j , the magnetic field is (equation 11.152 of [21], translated and rotated)

$$\vec{B}_j(0, t) = \begin{bmatrix} y \\ -x \\ 0 \end{bmatrix} \frac{\mu_0 e \gamma v}{4\pi(r_{\perp}^2 + \gamma^2 v^2 (t - t_j)^2)^{3/2}} \quad (3)$$

where $r_{\perp} = |\vec{r}_{\perp}|$ is the minimal distance between the single electron and the quantum system (impact parameter). We consider an ensemble of electrons with a Poissonian distribution in time and a Gaussian distribution in transverse dimensions that is initially velocity modulated, which leads to bunching. The results of a numerical simulation of the electron beam's magnetic field for experimentally relevant parameters are shown in Fig.2 (see Sec.3 of SM [14] for details).

For strong currents and large distances d on the order of micro-meters, the resulting magnetic field can be described as an ensemble averaged field with additional

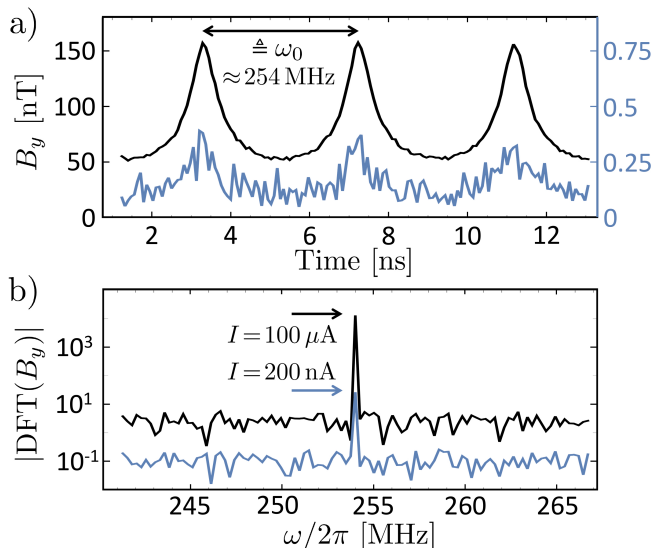


FIG. 2. a) Numerical simulation of the magnetic field strength B_y of a transversally Gaussian and temporally Poissonian current modulated electron beam as could be created in a klystron with bunching parameter $r_b \approx 0.5$. The waist radius is $w = 50 \mu\text{m}$ and the distance to the center of the beam is $d = 250 \mu\text{m}$. The plots show the cases of currents of 200 nA (blue plot, corresponding to about ~ 5000 electrons per period) and $100 \mu\text{A}$ (black plot, corresponding to ~ 250000 electrons per period). The electrons possess a kinetic energy of 18 keV and the base frequency of the modulated electron beam is 254 MHz. It can be seen that the relative strength of shot noise is decreased significantly for the $100 \mu\text{A}$ beam in comparison to the weaker 200 nA beam.

b) Fourier limited linewidth: discrete Fourier transform of the magnetic field strength B_y with the same parameters as in (a); 200 nA (blue plot) and $100 \mu\text{A}$ (black plot) evaluated for 10^3 periods. It can be seen that a decrease in current leads to a decrease in the signal to noise ratio but does not affect the linewidth of the modulation.

noise. In the supplement, we derive the average spectrum of the magnetic field oscillations and its variance, which has the expected signature of shot noise (see Sec.4 and Sec.5 of SM [14]). In particular, this noise appears as a homogeneous noise floor in the Fourier transform and does not modify the linewidth of coherent oscillations of the magnetic field. The averaged magnetic field has distinct spectral lines at the same frequencies as the spectrum of the beam's current modulation (see Sec.4 SM [14]), that is, the base frequency and higher harmonics [11, 22]. Furthermore, for $d > 2w$, the average magnetic field of a Gaussian beam can be well approximated by that due to an infinitely thin beam. If $d \ll \gamma\lambda_0$ and $d \ll \gamma l$, the magnetic field is approximately proportional to the current at the z -coordinate of the quantum system (see Sec.6 SM [14]). Based on the classical description of the magnetic near field due the electron beam, we can model the response of the quantum system.

Dynamics of the quantum system – We split the electromagnetic field into the near field of the electrons, and the radiation field considered to be initially free of excitations. The radiation field leads to damping via spontaneous emission (Sec.7 of SM [14]). We model the internal degrees of freedom of the quantum system as a two level system and describe the time evolution of its density matrix ρ with the optical Bloch equations (see Sec.4 of [23] and Sec.7 of SM [14])

$$0 = \left(\frac{d}{dt} - \begin{bmatrix} -\Gamma_2 & 0 & \frac{i\tilde{T}_{ge}^*}{\hbar} & -\frac{i\tilde{T}_{ge}^*}{\hbar} \\ 0 & -\Gamma_2 & -\frac{i\tilde{T}_{ge}}{\hbar} & \frac{i\tilde{T}_{ge}}{\hbar} \\ \frac{i\tilde{T}_{ge}}{\hbar} & -\frac{i\tilde{T}_{ge}^*}{\hbar} & -\Gamma_1 & 0 \\ -\frac{i\tilde{T}_{ge}}{\hbar} & \frac{i\tilde{T}_{ge}^*}{\hbar} & \Gamma_1 & 0 \end{bmatrix} \right) \begin{bmatrix} \tilde{\rho}_{eg} \\ \tilde{\rho}_{ge} \\ \tilde{\rho}_{ee} \\ \tilde{\rho}_{gg} \end{bmatrix} \quad (4)$$

We have defined $\tilde{\rho}$ as the density matrix ρ in the rotating frame with respect to the transition frequency ω_0 (e for excited and g for ground state) with components $\tilde{\rho}_{ee} = \rho_{ee}$, $\tilde{\rho}_{gg} = \rho_{gg}$, $\tilde{\rho}_{ge} = \rho_{ge}e^{-i\omega_0 t}$ and $\tilde{\rho}_{eg} = \rho_{eg}e^{i\omega_0 t}$. Furthermore, $\tilde{T}_{ge} = e^{-i\omega_0 t} \langle g | \hat{H}_{\text{int}} | e \rangle$ is the time dependent transition matrix element in the rotating frame. The rate Γ_1 incorporates the damping of the population inversion $\tilde{\rho}_{ee} - \tilde{\rho}_{gg}$ and Γ_2 is the decoherence rate.

For the case of a modulated current with small fluctuations relative to the mean (e.g. shot noise, modulation phase noise), and if resonance is assumed, the rotating wave approximation can be applied and \tilde{T}_{ge}^* is replaced by $-\hbar\Omega/2$, where Ω is the Rabi frequency given by the amplitude of the resonant oscillating component of $\langle g | H_{\text{int}} | e \rangle / \hbar$. The finite spectral linewidth of the near-field of the electron beam, represented by small phase fluctuations, leads to dephasing. This result has been derived for the interaction of atoms with laser light in [24–29], and can be applied immediately to our case due to the equivalence of the interaction Hamiltonian. One finds that the components of the density matrix co-rotated with the phase noise and averaged over its representations fulfill the optical Bloch equations with a modified decoherence constant $\tilde{\Gamma}_2 = \Gamma_2 + b$, where b is related to the Full Width at Half Maximum (FWHM) linewidth $\delta\omega$ of the modulation as $b = \delta\omega/2$ (see Sec.7 of SM [14]).

Using properties of integro-differential equations with short correlation times [30], it can be shown that shot noise leads to extra damping and decoherence terms entering the optical Bloch equations in a similar way as the rates Γ_1 , Γ_2 and b (see Sec.10 SM [14]). The additional terms are proportional to the pre-factor in the auto-covariance of the magnetic field and can be neglected if they are much smaller than the average Rabi frequency. Fortunately, this is the case for all sets of parameters within the scope of our proposal (see Sec.10 SM [14]) and we find that we can ignore shot noise. In the following, we will discuss two specific examples of quantum systems that can be driven based on our proposal.

Example 1: Driving ground state hyperfine transitions in alkali atoms – Alkali atoms, for example Li, K, and Rb, are especially well suited for a first demonstration of our scheme due to the easily accessible hydrogen-like level structure and two stable and easily detectable ground state hyperfine levels separated by a transition in the microwave range. Furthermore, ground state hyperfine transitions have a sufficiently narrow linewidth (long life time) and are spectrally sufficiently distinct to ensure that only one of the lines in the spectrum of the beam modulation is on resonance with the transition, and Condition 2 is fulfilled. In the following, we consider ^{41}K as a specific example. The nuclear spin of ^{41}K is $3/2$, and therefore its $4^2S_{1/2}$ ground state level splits into the hyperfine levels $F = 1$ and $F = 2$, where F indicates the total angular momentum. The transition $F = 1 \leftrightarrow F = 2$ has a frequency of ~ 254 MHz and is therefore easily accessible with low frequency MW-electronics. For the following, we restrict our considerations to the transition $F = 1, m_F = 0 \leftrightarrow F = 2, m_F = 0$, where m_F denotes the Zeeman sublevels. Considering the y -direction as the quantization axis, we find $\tilde{T}_{ge} \approx -e^{-i\omega_0 t} g_S \mu_B B_y / 2$, where g_S is the electron's gyromagnetic ratio and μ_B is the Bohr magneton. The resulting Rabi frequency is $\Omega \approx g_S \mu_B B_y / 2\hbar$, where B_y is the amplitude of the resonant component of the beam modulation (see [31] and Sec.8 SM [14]). We assume that the atom is initially in the hyperfine state $F = 2$. Furthermore, we consider an optically cooled and trapped ^{41}K atom [32] (which can be, in principle, controlled even on the nm scale using similar techniques as used for ^{39}K in [33] or for ^{87}Rb in [34]). The change of the internal state of the atom will be accompanied by a recoil equivalent in absolute value to the momentum transfer to the electron. The order of magnitude of this momentum transfer is that of the longitudinal momentum shift $\delta p_z = \hbar\omega_0/v \sim 10^{-33}$ kg m/s, which corresponds to a velocity change of the atom $\delta v_a \sim 10^{-8}$ m/s. Therefore, the atom can be considered to be stationary on the time scale of the Rabi oscillation. We consider an electron beam waist of $w = 50 \mu\text{m}$, kinetic energy of 18 keV, average current $I_0 = 100 \mu\text{A}$ and bunching parameter $r_b = 0.5$ corresponding to a resonant current modulation at the base frequency ω_0 of amplitude $2I_0 J_1(r_b) \sim 50 \mu\text{A}$ (where J_1 is the Bessel function of the first kind), and we assume $d = 250 \mu\text{m}$ between the atom and the beam center. The spectral linewidth of klystrons is mainly limited by technical noise [35]; as a conservative estimate we consider $\Delta\omega/\omega_0 = 10^{-7}$. In the case under consideration, this leads to a beam modulation spectral line width of about 25 Hz.

Plots of the hyperfine state response due to a modulated electron beam (see Sec.11 SM [14]) based on numerical evaluation of the optical Bloch equations can be found in Fig.3a. Several Rabi oscillations of the hyperfine states are clearly visible. The origin of the decay of coherence is the beam modulation spectral line width. Incoher-

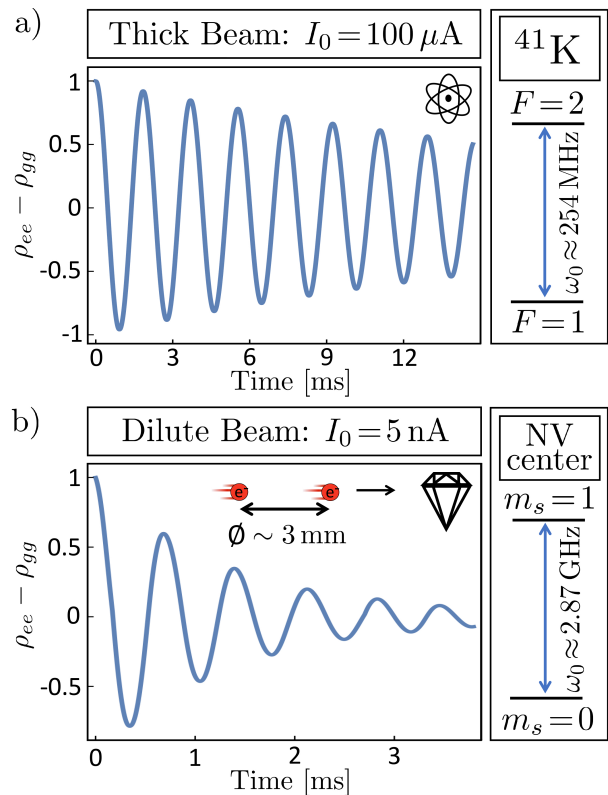


FIG. 3. Plot a) shows the time-evolution of the inversion for the transition $F = 1, m_F = 0 \leftrightarrow F = 2, m_F = 0$ for ^{41}K at a distance $d = 250 \mu\text{m}$ from the center of an electron beam of waist $w = 50 \mu\text{m}$, current $100 \mu\text{A}$, bunching parameter $r_b = 0.5$, $E_{\text{kin}} = 18$ keV, FWHM linewidth of the electron beam modulation $b/\pi = 25$ Hz and $\Gamma_1 = 2\Gamma_2 \ll b$.

Plot b) shows the time-evolution of the inversion for the transition $m_s = 0 \leftrightarrow m_s = 1$ in the 3A_2 -state of an NV center at distance $d = 5$ nm from a beam of waist $w = 1$ nm, current of 5 nA, $E_{\text{kin}} = 30$ keV and bunching parameter $r_b \approx 0.5$. We set $1/\Gamma_1 = T_1 = 6$ ms, $1/\Gamma_2 = T_2 = 3$ ms and the FWHM linewidth of the electron beam modulation $b/\pi = 300$ Hz.

ent scattering events happen on much longer time scales than the Rabi period. We estimate the scattering probability using the total scattering cross section (comprising ionization, elastic and inelastic scattering). For potassium atoms exposed to an 18 keV electron beam, we find $\sigma_{\text{tot}} \approx 1.5 \cdot 10^{-17} \text{cm}^2$, extrapolated from [36]. The current density j of a Gaussian beam at $5w$ would theoretically lead to a negligible scattering rate $\sigma_{\text{tot}} j/e$, where e is the elementary charge. Even if a remaining current density of 0.1% of the peak value is assumed as a conservative estimate, the scattering probability only amounts to less than $\sim 1\%$ after 20 ms.

Example 2: NV centers in nano diamonds – In the following, we will consider Nitrogen Vacancy (NV) centers in nano-diamonds as an example of the case where nanometer distances between an electron beam and a quantum system can be achieved. In this situation, the magnetic near field of the electron beam consists of distinct

spikes due to the well separated electrons. Therefore, we cannot use the expected value for the magnetic field in the optical Bloch equations. Instead, we simulate the effect of the magnetic field of each electron separately. We focus on the transition between the 3A_2 ground state magnetic sublevels $m_s = 0$ and $m_s = 1$ that are split by $\omega_0 = 2.87$ GHz [37]. The $m_s = -1$ sublevel is well separated from the $m_s = 1$ sublevel by at least ~ 4 MHz [38] such that the transition $m_s = 0 \leftrightarrow m_s = 1$ can be individually addressed and easily optically detected. We consider the x -direction as the quantization direction, with the magnetic field oriented in the y -direction; we find that the transition matrix element is given by $\tilde{T}_{ge} = e^{-i\omega_0 t} g_s \mu_B B_y / \sqrt{2}$ (see Sec.9 SM [14]). This transition exhibits coherence times T_2 from $600 \mu\text{s}$ [39] up to 600 ms ([40] using a dynamical decoupling pulse sequence), which is the main decay channel for the Rabi oscillations of the NV center (see Fig.3b). As the electron beam source, we consider a standard scanning electron microscope with a modulated electron beam current generating a beam waist of $w = 1$ nm at 30 keV, a beam current of 5 nA (~ 11 electrons per modulation period) and a bunching parameter $r_b = 0.5$ directed at a distance of 5 nm next to an NV center, for example embedded in a free standing nanostructure [41]. A simulation of the expected level response is presented in Fig.3b. Several Rabi oscillations are clearly visible for this example, primarily damped by the intrinsic rates $\Gamma_2 = 1/T_2$ and $\Gamma_1 = 1/T_1$. To reduce unwanted effects due to electrons scattering on the diamond structure [42] to a negligible level, the electron beam intensity at the position of the NV center should be reduced by a factor of 10^{-7} compared to its maximum. This can be achieved for a Gaussian beam at $5w$. At this intensity, on average less than one electron scatters within a radius of 1 nm next to the NV center every period of the Rabi oscillation.

Conclusions and Discussions – We have shown that transitions of quantum systems can be selectively addressed by the classical electromagnetic near field of an intensity modulated electron beam even on the nanoscale. We have proposed two specific setups based on a modulated beam realizable with current technology.

Research efforts to bring electron beam physics into the realm of coherent quantum dynamics have been mainly focused on the x-ray regime [43–47] and the optical regime [48–58]. In this work, we focused on current modulations in the microwave band which facilitates the experimental realization. Furthermore, microwave transitions of quantum systems are an important tool in quantum optics and quantum technologies [59, 60]. The proposed scheme can be beneficial for such applications as it would allow for nanometer scale resolution. Furthermore, our scheme may be applicable to novel development towards quantum computing, where several approaches use stable transitions in the MW range [59], or to coherently address single NV centers in a network of multiple NV

centers within a nano-diamond.

Employing the near field of modulated electron beams, it is possible to obtain strong electric and magnetic field gradients which enables the driving of higher multipole transitions of quantum systems. This could be used to target dipole-forbidden transitions, for example, to search for physics beyond the standard model [61].

Our scheme could be combined with scanning electron microscopes [62] to perform coherent spectroscopic investigations. A current modulated electron beam could be directed next to the region of interest, specific quantum transitions would be excited and the effect on the sample could be read out by an optical channel [63], or in future applications, by microwave sensors [64]. For an appropriately chosen distance to the sample, resonant driving leads to a significantly higher transition rate than the incoherent scattering effects (exemplified in Fig.3 by the quadratic increase of the transition probability with time, and therefore, number of electrons of the coherently driven evolution in contrast to the much lower, initially linear effect of incoherent scattering). Hence, this scheme could be utilized to investigate specimens with reduced electron dose.

ACKNOWLEDGEMENTS

We thank Holger Müller, Jörg Schmiedmayer, Peter Schattschneider, Thomas Schachinger, Hannes Matuschek, Philipp Thomas, Matthias Sonnleitner, Gregor Pieplow, Kiri Mochrie, Ralf Menzel, Francesco Intravaia, Igor Mazets, Matthias Kolb, Thomas Weigner, Michael Scheucher, Thomas Juffmann, Stephanie Manz, Arne Wickenbrock and Thomas Kiel for helpful remarks and discussions. DR and PH acknowledge the hospitality of the Erwin Schrödinger Institute in the framework of their research in team project. DR thanks the Humboldt Foundation and the Marie Skłodowska-Curie Actions IF program for support. PH thanks the Austrian Science Fund (FWF): J3680, Y1121. This project was supported by the ESQ-Discovery Program 2019 ”Quantum Klystron (QUAK)”.

* dennis.raetzel@physik.hu-berlin.de

† philipp.haslinger@tuwien.ac.at

- [1] V. Giovannetti, S. Lloyd, and L. Maccone, Quantum metrology, *Phys. Rev. Lett.* **96**, 010401 (2006).
- [2] R. H. Parker, C. Yu, W. Zhong, B. Estey, and H. Müller, Measurement of the fine-structure constant as a test of the standard model, *Science* **360**, 191 (2018).
- [3] C. Monroe, Quantum information processing with atoms and photons, *Nature* **416**, 238 (2002).
- [4] A. Imamog, D. D. Awschalom, G. Burkard, D. P. DiVincenzo, D. Loss, M. Sherwin, A. Small, *et al.*, Quantum

- information processing using quantum dot spins and cavity qed, *Phys. Rev. Lett.* **83**, 4204 (1999).
- [5] B. Hecht, B. Sick, U. P. Wild, V. Deckert, R. Zenobi, O. J. F. Martin, and D. W. Pohl, Scanning near-field optical microscopy with aperture probes: Fundamentals and applications, *The Journal of Chemical Physics* **112**, 7761 (2000).
- [6] S. Nie and S. R. Emory, Probing single molecules and single nanoparticles by surface-enhanced raman scattering, *Science* **275**, 1102 (1997).
- [7] L. Reimer and H. Kohl, *Transmission Electron Microscopy* (Springer, 2008).
- [8] R. F. Egerton, *Electron energy-loss spectroscopy in the electron microscope* (Springer, 2011).
- [9] S. Meuret, L. H. Tizei, T. Cazimajou, R. Bourrellier, H. C. Chang, F. Treussart, and M. Kociak, Photon bunching in cathodoluminescence, *Physical Review Letters* **114** (2015).
- [10] R. H. Varian and S. F. Varian, A high frequency amplifier and oscillator, *Journal of Applied Physics* **10**, 140 (1939).
- [11] A. Gilmour, *Klystrons, Traveling Wave Tubes, Magnetrons, Crossed-Field Amplifiers, and Gyrotrons* (Artech House, 2011).
- [12] L. D. Favro, D. M. Fradkin, and P. K. Kuo, Energy transfer via scattering of a coherent modulated electron beam, *Phys. Rev. D* **3**, 2934 (1971).
- [13] A. Gover and A. Yariv, Free-electron-bound-electron resonant interaction, *Phys. Rev. Lett.* **124**, 064801 (2020).
- [14] *Supplemental Material*.
- [15] P. Schattschneider, *Fundamentals of inelastic electron scattering* (Springer Science & Business Media, 2012).
- [16] J. Gadzuk, Many-body tunneling-theory approach to field emission of electrons from solids, *Surface Science* **15**, 466 (1969).
- [17] K. Nagaoka, T. Yamashita, S. Uchiyama, M. Yamada, H. Fujii, and C. Oshima, Monochromatic electron emission from the macroscopic quantum state of a superconductor, *Nature* **396**, 557 (1998).
- [18] F. Hasselbach, Progress in electron- and ion-interferometry, *Reports on Progress in Physics* **73**, 016101 (2009).
- [19] H. Ferwerda, *Coherence of illumination in electron microscopy* (Springer, 1980).
- [20] M. P. Silverman, *Quantum superposition: counterintuitive consequences of coherence, entanglement, and interference* (Springer Science & Business Media, 2008).
- [21] J. D. Jackson, *Classical electrodynamics* (Wiley, New York, 1999).
- [22] D. L. Webster, Cathode-ray bunching, *Journal of Applied Physics* **10**, 501 (1939).
- [23] P. Meystre and M. Sargent, *Elements of quantum optics* (Springer Science & Business Media, 2007).
- [24] P. Zoller, Atomic relaxation and resonance fluorescence in intensity and phase-fluctuating laser light, *Journal of Physics B* **11**, 2825 (1978).
- [25] J. Eberly, Atomic relaxation in the presence of intense partially coherent radiation fields, *Phys. Rev. Lett.* **37**, 1387 (1976).
- [26] P. L. Knight and P. W. Milonni, The rabi frequency in optical spectra, *Physics Reports* **66**, 21 (1980).
- [27] H. Kimble and L. Mandel, Resonance fluorescence with excitation of finite bandwidth, *Physical Review A* **15**, 689 (1977).
- [28] G. Agarwal, Exact solution for the influence of laser temporal fluctuations on resonance fluorescence, *Phys. Rev. Lett.* **37**, 1383 (1976).
- [29] J. Mostowski and K. Rzazewski, Rabi oscillations in a partially coherent field, *Zeitschrift für Physik B Condensed Matter* **39**, 183 (1980).
- [30] N. G. Van Kampen, Stochastic differential equations, *Physics reports* **24**, 171 (1976).
- [31] T. G. Tiecke, Properties of potassium, Thesis (2010).
- [32] M. Landini, S. Roy, L. Carcagnì, D. Trypogeorgos, M. Fattori, M. Inguscio, and G. Modugno, Sub-doppler laser cooling of potassium atoms, *Physical Review A* **84**, 43432 (2011).
- [33] L. W. Cheuk, M. A. Nichols, M. Okan, T. Gersdorf, V. V. Ramasesh, W. S. Bakr, T. Lompe, and M. W. Zwierlein, Quantum-gas microscope for fermionic atoms, *Physical Review Letters* **114**, 193001 (2015).
- [34] T. Gericke, P. Wrtz, D. Reitz, T. Langen, and H. Ott, High-resolution scanning electron microscopy of an ultracold quantum gas, *Nature Physics* **4**, 949 (2008).
- [35] R. B. Hemphill, Thesis, klystron-frequency stabilization for a paramagnetic-resonance spectrometer (1960).
- [36] M. Inokuti, Inelastic collisions of fast charged particles with atoms and molecules - the bethe theory revisited, *Rev. Mod. Phys.* **43**, 297 (1971).
- [37] M. W. Doherty, N. B. Manson, P. Delaney, and L. C. L. Hollenberg, The negatively charged nitrogen-vacancy centre in diamond: the electronic solution, *New Journal of Physics* **13**, 025019 (2011).
- [38] H. Zheng, J. Xu, G. Z. Iwata, T. Lenz, J. Michl, B. Yavkin, K. Nakamura, H. Sumiya, T. Ohshima, J. Isoya, J. Wrachtrup, A. Wickenbrock, and D. Budker, Zero-field magnetometry based on nitrogen-vacancy ensembles in diamond, *Phys. Rev. Applied* **11**, 064068 (2019).
- [39] P. L. Stanwix, L. M. Pham, J. R. Maze, D. Le Sage, T. K. Yeung, P. Cappellaro, P. R. Hemmer, A. Yacoby, M. D. Lukin, and R. L. Walsworth, Coherence of nitrogen-vacancy electronic spin ensembles in diamond, *Physical Review B* **82**, 201201 (2010).
- [40] N. Bar-Gill, L. M. Pham, A. Jarmola, D. Budker, and R. L. Walsworth, Solid-state electronic spin coherence time approaching one second, *Nature Communications* **4**, 1743 (2013).
- [41] M. Batzer, B. Shields, E. Neu, C. Widmann, C. Giese, C. Nebel, and P. Maletinsky, Single crystal diamond pyramids for applications in nanoscale quantum sensing, *Optical Materials Express* **10**, 492 (2020).
- [42] S. Tanuma, C. J. Powell, and D. R. Penn, Calculations of electron inelastic mean free paths. IX. Data for 41 elemental solids over the 50 eV to 30 keV range, *Surface and Interface Analysis* **43**, 689 (2011).
- [43] R. Bonifacio, N. Piovella, G. R. M. Robb, and A. Schiavi, Quantum regime of free electron lasers starting from noise, *Phys. Rev. ST Accel. Beams* **9**, 090701 (2006).
- [44] A. Debus, K. Steiniger, P. Kling, C. M. Carmesin, and R. Sauerbrey, Realizing quantum free-electron lasers: a critical analysis of experimental challenges and theoretical limits, *Physica Scripta* **94**, 074001 (2019).
- [45] G. Dattoli and H. Fares, The gaussian integration method of the schrödinger equation and quantum 1-d theory of low gain free electron laser, *Journal of Mathematical Physics* **60**, 042101 (2019).

- [46] P. Kling, E. Giese, R. Endrich, P. Preiss, R. Sauerbrey, and W. P. Schleich, What defines the quantum regime of the free-electron laser?, *New Journal of Physics* **17**, 123019 (2015).
- [47] Y. Yang, A. Massuda, C. Roques-Carnes, S. E. Kooi, T. Christensen, S. G. Johnson, J. D. Joannopoulos, O. D. Miller, I. Kaminer, and M. Soljačić, Maximal spontaneous photon emission and energy loss from free electrons, *Nature Physics* **14**, 894 (2018).
- [48] H. Batelaan, Colloquium: Illuminating the kapitza-dirac effect with electron matter optics, *Reviews of Modern Physics* **79**, 929 (2007).
- [49] G. de Abajo, Colloquium: Light scattering by particle and hole arrays, *Reviews of Modern Physics* **79**, 12671290 (2007).
- [50] M. Krüger, M. Schenk, and P. Hommelhoff, Attosecond control of electrons emitted from a nanoscale metal tip, *Nature* **475**, 78 (2011).
- [51] A. Yurtsever, v. d. R. M. Veen, and A. H. Zewail, Subparticle ultrafast spectrum imaging in 4d electron microscopy, *Science* **335**, 59 (2012).
- [52] F. O. Kirchner, A. Gliserin, F. Krausz, and P. Baum, Laser streaking of free electrons at 25 keV, *Nature Photonics* **8**, 52 (2014).
- [53] A. Feist, K. E. Echternkamp, J. Schauss, V. S. Yalunin, S. Schfer, and C. Ropers, Quantum coherent optical phase modulation in an ultrafast transmission electron microscope, *Nature* **521**, 200 (2015).
- [54] L. Piazza, T. T. Lummen, E. Quionez, Y. Murooka, B. W. Reed, B. Barwick, and F. Carbone, Simultaneous observation of the quantization and the interference pattern of a plasmonic near-field, *Nature Communications* **6**, 6407 (2015).
- [55] K. E. Echternkamp, A. Feist, S. Schfer, and C. Ropers, Ramsey-type phase control of free-electron beams, *Nature Physics* **12**, 1000 (2016).
- [56] A. Gover and Y. Pan, Dimension-dependent stimulated radiative interaction of a single electron quantum wavepacket, *Physics Letters A* **382**, 1550 (2018).
- [57] O. Kfir, Entanglements of electrons and cavity photons in the strong-coupling regime, *Phys. Rev. Lett.* **123**, 103602 (2019).
- [58] A. Polman, M. Kociak, and F. J. Garca de Abajo, Electron-beam spectroscopy for nanophotonics, *Nature Materials* **18**, 1158 (2019).
- [59] C. D. Bruzewicz, J. Chiaverini, R. McConnell, and J. M. Sage, Trapped-ion quantum computing: Progress and challenges, *Applied Physics Reviews* **6**, 021314 (2019).
- [60] P. T. Callaghan, *Principles of nuclear magnetic resonance microscopy* (Clarendon Press, 1993).
- [61] V. F. Ezhov, M. G. Kozlov, G. B. Krygin, V. A. Ryzhov, and V. L. Ryabov, On the Possibility of Measuring the Anapole Moment of Potassium Atom, *Technical Physics Letters* **30**, 917 (2004).
- [62] W. Verhoeven, J. F. van Rens, E. R. Kieft, P. H. Mutsaers, and O. J. Luiten, High quality ultrafast transmission electron microscopy using resonant microwave cavities, *Ultramicroscopy* **188**, 85 (2018).
- [63] M. W. Doherty, N. B. Manson, P. Delaney, F. Jelezko, J. Wrachtrup, and L. C. Hollenberg, The nitrogen-vacancy colour centre in diamond, *Physics Reports* **528**, 145 (2013).
- [64] J. Anders and J. G. Korvink, *Micro and Nano Scale NMR*, *Advanced Micro and Nanosystems* (Wiley-VCH, 2018).
- [65] V. B. Berestetskii, E. M. Lifshitz, and L. P. Pitaevskii, *Quantum electrodynamics*, Vol. 4 (Butterworth-Heinemann, 1982).
- [66] L. L. Landau and E. M. Lifshitz, *A shorter course of theoretical physics - Volume 2 Quantum mechanics* (Pergamon Press, 2011).
- [67] C. Itzykson and J.-B. Zuber, *Quantum field theory* (Courier Corporation, 2012).
- [68] P. Farago and R. Sillitto, 27. the quantum theory of the klystron and the modulation of electron beams at optical frequencies, *Proceedings of the Royal Society of Edinburgh Section A: Mathematics* **71**, 305 (1974).
- [69] H. C. Tijms, *A first course in stochastic models* (John Wiley and sons, 2003).
- [70] N. G. Van Kampen, *Stochastic processes in physics and chemistry*, Vol. 1 (Elsevier, 1992).
- [71] J. D. A. Wood, D. A. Broadway, L. T. Hall, A. Stacey, D. A. Simpson, J.-P. Tetienne, and L. C. L. Hollenberg, Wide-band nanoscale magnetic resonance spectroscopy using quantum relaxation of a single spin in diamond, *Phys. Rev. B* **94**, 155402 (2016).

SUPPLEMENTAL MATERIAL

1. BACK-ACTION AND DECOHERENCE

If the change of state of the electron due to back-action is in principle detectable, decoherence occurs in the reduced state of the quantum system. Here, we analyze this effect. We assume that the quantum system's dimensions are much smaller than its distance to the center of the electron beam d and the modulation wave length $\lambda_0 = 2\pi v/\omega_0$, where v is the average velocity of the electrons and ω_0 is the radian frequency of the modulation and the transition frequency of the quantum system. Thus, we can consider the quantum system as point-like. Furthermore, we consider an initial Gaussian matter-wave packet of longitudinal size much smaller than λ_0 such that the beam modulation is not on the level of the single electron wave function but corresponds to correlations between electrons. The transversal width of the Gaussian matter-wave packet is bound from above by the focal width of the beam as $\Delta r_\perp < w/2$ and in our specific implementation, we consider $d \sim 5w$. This implies that $d \gg \Delta r_\perp$ and the amplitude of the electron wave function is approximately zero at the position of the quantum system.

The magnetic field at the position of the quantum system induced by a beam-electron is proportional to its orbital angular momentum with respect to this position ($\propto d p_z$). When seen as a magnetic dipole, the spin of the beam-electron induces a magnetic field proportional to the spin angular momentum ($\propto \hbar/2$). We consider distances d much larger than the de Broglie wavelength of the beam electrons, and therefore $1 \ll d/\lambda_{\text{dB}} = d p_{z,0}/(2\pi\hbar)$, where $p_{z,0} = \gamma m v$ is the average momentum of the electrons in the beam. Thus, we can restrict our considerations to the coupling of the orbital angular momentum of the beam electrons to the quantum system and neglect the much smaller effect of their spin angular momentum. Hence, we describe the electron field as a charged scalar field normalized with the charge

$$Q(\psi, \psi') = i \int d^3r (\psi^* \partial_{ct} \psi' - (\partial_{ct} \psi^*) \psi'), \quad (5)$$

such that $Q(\psi_p, \psi_{p'}) = (2\pi\hbar)^3 \delta^{(3)}(\vec{p} - \vec{p}')$.

We assume that the electromagnetic field stays in the vacuum throughout the process and that the quantum system is initially in the excited state $|e\rangle$ and consider an interaction with an electron in the state

$$|\text{in}\rangle_{\text{el}} = \int \frac{d^3p}{(2\pi\hbar)^3} \phi_{\text{in}}(\vec{p}) |\vec{p}\rangle \quad (6)$$

where $\phi_{\text{in}}(\vec{p})$ is the single electron wave function in the momentum representation, and $|\vec{p}\rangle$ is a momentum state defined such that $\psi_p(\vec{r}, 0) = \langle \vec{r} | \vec{p} \rangle = e^{i\vec{p}\cdot\vec{r}/\hbar} / \sqrt{2\omega_p/c}$. To lowest order, after the electron and quantum system interact, the full state will be

$$|\text{out}\rangle = \sqrt{1 - P_{e \rightarrow g}} |e\rangle \otimes \int \frac{d^3p}{(2\pi\hbar)^3} \phi_{\text{in}}(\vec{p}) |\vec{p}\rangle + \sqrt{P_{e \rightarrow g}} |g\rangle \otimes \int \frac{d^3p}{(2\pi\hbar)^3} \phi_{\text{scatt}}(\vec{p}) |\vec{p}\rangle, \quad (7)$$

where $P_{e \rightarrow g}$ is the probability for the transition from the excited to the ground state and we define

$$\phi_{\text{scatt}}(\vec{p}, t) = (P_{e \rightarrow g})^{-1/2} \int \frac{d^3p'}{(2\pi\hbar)^3} \phi_{\text{in}}(\vec{p}') \mathcal{S}(\vec{p}, \vec{p}'), \quad (8)$$

where $\mathcal{S}(\vec{p}', \vec{p}) := \langle g, \vec{p}', \text{vac} | \hat{S}^{(2)} | e, \vec{p}, \text{vac} \rangle$ is the scattering matrix element for the transition from momentum \vec{p}' to \vec{p} in second order perturbation theory. The probability follows from

$$1 = \left| \int \frac{d^3p}{(2\pi\hbar)^3} \phi_{\text{scatt}}(\vec{p}) |\vec{p}\rangle \right|^2 = \int \frac{d^3p}{(2\pi\hbar)^3} |\phi_{\text{scatt}}(\vec{p})|^2 \quad (9)$$

$$= (P_{e \rightarrow g})^{-1} \int \frac{d^3p}{(2\pi\hbar)^3} \frac{d^3p'}{(2\pi\hbar)^3} \frac{d^3p''}{(2\pi\hbar)^3} \phi_{\text{in}}^*(\vec{p}') \mathcal{S}^*(\vec{p}, \vec{p}') \mathcal{S}(\vec{p}, \vec{p}'') \phi_{\text{in}}(\vec{p}''). \quad (10)$$

The driving process can only be coherent if the reduced density matrix

$$\varrho_a = \text{Tr}_{\text{el}}[|\text{out}\rangle\langle\text{out}|] \quad (11)$$

(with the partial trace taken over the electron Hilbert space) is close to that of a pure state. To this end, the overlap of the electron's in-state and its out-state ${}_{\text{el}}\langle\text{in}|\text{out}\rangle_{\text{el}}$ must be close to one. We only consider the positive energy

sector. Starting from the Fourier representation of wave functions

$$\psi_i(\vec{r}, t) = \int \frac{d^3p}{(2\pi\hbar)^3} \phi_i(\vec{p}) \frac{1}{\sqrt{2\omega_p/c}} e^{i\vec{p}\cdot\vec{r}/\hbar} e^{-i\omega_p t}, \quad (12)$$

where $\omega_p = c\sqrt{|\vec{p}|^2 + m^2c^2}/\hbar$, we find that the inner product in momentum space becomes

$$\langle \psi_1, \psi_2 \rangle = \frac{i}{c} \int d^3r (\psi_1^*(\vec{r}, t) \partial_t \psi_2(\vec{r}, t) - \psi_2(\vec{r}, t) \partial_t \psi_1^*(\vec{r}, t)) = \int \frac{d^3p}{(2\pi\hbar)^3} \phi_1^*(\vec{p}) \phi_2(\vec{p}). \quad (13)$$

Therefore, we have to evaluate

$$\text{el} \langle \text{in} | \text{out} \rangle_{\text{el}} = \frac{1}{\sqrt{P_{e \rightarrow g}}} \int \frac{d^3p}{(2\pi\hbar)^3} \frac{d^3p'}{(2\pi\hbar)^3} \phi_{\text{in}}^*(\vec{p}) \phi_{\text{in}}(\vec{p}') \mathcal{S}(\vec{p}, \vec{p}'). \quad (14)$$

The scattering matrix element

We have for the S-matrix (see Chapter VIII of [65] or 104 of [66] for details)

$$\hat{S} = \mathcal{T} \exp \left(-\frac{i}{\hbar c} \int d^4x \hat{J}^\mu \hat{A}_\mu \right), \quad (15)$$

where \mathcal{T} denotes time ordering, \hat{J}^μ contains all of the currents of charged particles and \hat{A}_μ is the electromagnetic 4-potential operator. The lowest order interaction term for our process occurs at the second order, for which we find

$$\hat{S}^{(2)} = -\frac{1}{2(\hbar c)^2} \int d^4x \int d^4x' \mathcal{T} \left(\hat{J}^\mu(x) \hat{J}^\nu(x') \right) \mathcal{T} \left(\hat{A}_\mu(x) \hat{A}_\nu(x') \right). \quad (16)$$

For the process under consideration, the electromagnetic field stays in the vacuum state and we use

$$\langle \text{vac} | \mathcal{T} \left(\hat{A}_\mu(x) \hat{A}_\nu(x') \right) | \text{vac} \rangle = i D_{\mu\nu}^{\text{F}}(x - x'), \quad (17)$$

where $D_{\mu\nu}^{\text{F}}(x - x')$ is the Feynman propagator of the electromagnetic field. We are considering a regime where the quantum system only changes its internal state and the free electrons remain free, that is, we are neglecting any violent effects such as ionization. Then, the charged current operator can be split into the current operator of the free electron and that of the quantum system as

$$\hat{J}^\mu(x) = [\hat{J}^{\text{el}}(x)]^\mu + [\hat{J}^{\text{qs}}(x)]^\mu \quad (18)$$

and we obtain

$$\mathcal{S}(\vec{p}, \vec{p}') = \langle g, \vec{p}' | \hat{S}^{(2)} | e, \vec{p}, \text{vac} \rangle = -\frac{i}{(\hbar c)^2} \int d^4x d^4x' [J_{p \rightarrow p'}^{\text{el}}(x)]^\mu D_{\mu\nu}^{\text{F}}(x - x') [J_{e \rightarrow g}^{\text{qs}}(x')]^\nu, \quad (19)$$

where $J_{p \rightarrow p'}^{\text{el}}(x)$ is the transition current of the free electron and $J_{e \rightarrow g}^{\text{qs}}(x')$ is the transition current of the quantum system. We consider the Feynman propagator in the Coulomb gauge such that only spatial components do not vanish:

$$D_{ij}^{\text{F}}(x - x') = -\mu_0 \hbar^3 c \lim_{\epsilon \rightarrow 0^+} \int \frac{d^4q}{(2\pi\hbar)^4} e^{i\vec{q}\cdot(\vec{r}-\vec{r}')/\hbar} e^{-iq_0 c(t-t')/\hbar} \frac{1}{q_0^2 - |\vec{q}|^2 + i\epsilon} \left(\delta_{ij} - \frac{q_i q_j}{q_0^2} \right). \quad (20)$$

Therefore, we can restrict our considerations to the spatial components of the transition current. We describe the free electron as a charged scalar field with current

$$\vec{J}_{p \rightarrow p'}^{\text{el}} = iec (\psi_{p'}^* \nabla \psi_p - (\nabla \psi_{p'}^*) \psi_p) = -\frac{ec^2}{2\hbar \sqrt{\omega_p \omega_{p'}}} (\vec{p}' + \vec{p}) e^{-i(\vec{p}' - \vec{p}) \cdot \vec{r} / \hbar} e^{i(\omega_{p'} - \omega_p)t} \quad (21)$$

(we remark that the quantization volume is omitted throughout the calculations, so $\vec{J}_{p \rightarrow p'}^{\text{el}}$ has the dimensions of a current instead of a current density). To describe the schemes proposed in this work, we restrict our considerations to magnetic dipole transitions of the quantum system. Furthermore, we assume that the quantum system is much heavier

than the electrons (e.g. $m_e/m_{41K} \sim 10^{-5}$ for our first example and much smaller for the NV-center in diamond) such that we can ignore the momentum recoil on the quantum system for this calculation. In this case, the spatial wave function of the quantum system is always unchanged to a good approximation. Then, the transition current of the quantum system can be approximated as that of a point-like magnetic dipole (see page 79 of [67])

$$\vec{J}_{e \rightarrow g}^{\text{qs}}(x) = -e^{-i\omega_0 t} \vec{\mu} \times \nabla \delta^{(3)}(\vec{r}), \quad (22)$$

where $\vec{\mu}$ is the magnetic transition dipole moment. Partial integration and execution of the Fourier transforms leads to

$$\begin{aligned} \mathcal{S}(\vec{p}, \vec{p}') &= i \frac{e\mu_0 c}{2\sqrt{\omega_p \omega_{p'}}} \int \frac{d^4 q}{(2\pi\hbar)^4} \int d^4 x d^4 x' (\vec{p}' + \vec{p})^i e^{-i(\vec{p}' - \vec{p}) \cdot \vec{r} / \hbar} e^{i(\omega_{p'} - \omega_p) t} \\ &\quad e^{i\vec{q} \cdot (\vec{r} - \vec{x}') / \hbar} e^{-iq_0 c(t-t') / \hbar} \lim_{\epsilon \rightarrow 0^+} \frac{1}{q_0^2 - |\vec{q}|^2 + i\epsilon} \left(\delta_{ij} - \frac{q_i q_j}{q_0^2} \right) e^{-i\omega_0 t'} \epsilon^{jkl} \mu_k \nabla_l \delta^{(3)}(\vec{r}') \\ &= i \frac{e\mu_0 c}{2\sqrt{\omega_p \omega_{p'}}} \int \frac{d^3 q}{(2\pi\hbar)^3} \int d^4 x d^3 r' (\vec{p}' + \vec{p})^i e^{-i(\vec{p}' - \vec{p}) \cdot \vec{r} / \hbar} e^{i(\omega_{p'} - \omega_p - \omega_0) t} \\ &\quad e^{i\vec{q} \cdot (\vec{r} - \vec{x}') / \hbar} \lim_{\epsilon \rightarrow 0^+} \frac{1}{(\hbar\omega_0/c)^2 - |\vec{q}|^2 + i\epsilon} \left(\delta_{ij} - \frac{q_i q_j}{(\hbar\omega_0/c)^2} \right) \epsilon^{jkl} \mu_k \nabla_l \delta^{(3)}(\vec{r}') \\ &= i \frac{e\mu_0 c}{2\sqrt{\omega_p \omega_{p'}}} \int \frac{d^3 q}{(2\pi\hbar)^3} \int d^3 r d^3 r' (\vec{p}' + \vec{p})^i e^{-i(\vec{p}' - \vec{p}) \cdot \vec{r} / \hbar} 2\pi\delta(\omega_{p'} - \omega_p - \omega_0) \\ &\quad e^{i\vec{q} \cdot (\vec{r} - \vec{r}') / \hbar} \lim_{\epsilon \rightarrow 0^+} \frac{1}{(\hbar\omega_0/c)^2 - |\vec{q}|^2 + i\epsilon} \left(\delta_{ij} - \frac{q_i q_j}{(\hbar\omega_0/c)^2} \right) \epsilon^{jkl} \mu_k \nabla_l \delta^{(3)}(\vec{r}') \\ &= i \frac{e\mu_0 c^2}{2\sqrt{\omega_p \omega_{p'}}} \int d^3 r' (\vec{p}' + \vec{p})^i 2\pi\delta(\omega_{p'} - \omega_p - \omega_0) \\ &\quad e^{-i(\vec{p}' - \vec{p}) \cdot \vec{x}' / \hbar} \lim_{\epsilon \rightarrow 0^+} \frac{1}{(\hbar\omega_0/c)^2 - |\vec{p}' - \vec{p}|^2 + i\epsilon} \left(\delta_{ij} - \frac{(\vec{p}' - \vec{p})_i (\vec{p}' - \vec{p})_j}{(\hbar\omega_0/c)^2} \right) \epsilon^{jkl} \mu_k \nabla_l \delta^{(3)}(\vec{r}') \\ &= -\frac{e\mu_0 c^2}{2\hbar\sqrt{\omega_p \omega_{p'}}} (\vec{p}' + \vec{p})^i 2\pi\delta(\omega_{p'} - \omega_p - \omega_0) \\ &\quad (\vec{p}' - \vec{p})_l \lim_{\epsilon \rightarrow 0^+} \frac{1}{(\hbar\omega_0/c)^2 - |\vec{p}' - \vec{p}|^2 + i\epsilon} \left(\delta_{ij} - \frac{(\vec{p}' - \vec{p})_i (\vec{p}' - \vec{p})_j}{(\hbar\omega_0/c)^2} \right) \epsilon^{jkl} \mu_k \\ &= -\frac{e\mu_0 c^2}{2\hbar\sqrt{\omega_p \omega_{p'}}} (\vec{p}' + \vec{p})_j (\vec{p}' - \vec{p})_l \epsilon^{jkl} \mu_k \lim_{\epsilon \rightarrow 0^+} \frac{1}{(\hbar\omega_0/c)^2 - |\vec{p}' - \vec{p}|^2 + i\epsilon} 2\pi\delta(\omega_{p'} - \omega_p - \omega_0). \end{aligned} \quad (23)$$

The scattered state

For the scattered state, we find

$$\begin{aligned} \bar{\phi}(\vec{p}') &:= \int \frac{d^3 p}{(2\pi\hbar)^3} \phi_{\text{in}}(\vec{p}) \mathcal{S}(\vec{p}, \vec{p}') \\ &= -\frac{e\mu_0 c^2}{2\hbar} \int \frac{d^3 p}{(2\pi\hbar)^3} \phi_{\text{in}}(\vec{p}) \frac{1}{\sqrt{\omega_p \omega_{p'}}} (\vec{p}' + \vec{p})_j (\vec{p}' - \vec{p})_l \epsilon^{jkl} \mu_k \\ &\quad \lim_{\epsilon \rightarrow 0^+} \left[\frac{1}{(\hbar\omega_0/c)^2 - |\vec{p}' - \vec{p}|^2 + i\epsilon} \right] 2\pi\delta(\omega_{p'} - \omega_p - \omega_0) \\ &= -\frac{e\mu_0 c^2}{\hbar} p'_j \int \frac{d^3 q}{(2\pi\hbar)^3} \phi_{\text{in}}(\vec{p}' - \vec{q}) \frac{1}{\sqrt{\omega_p \omega_{p'}}} q_l \epsilon^{jkl} \mu_k \lim_{\epsilon \rightarrow 0^+} \left[\frac{1}{(\hbar\omega_0/c)^2 - |\vec{q}|^2 + i\epsilon} \right] 2\pi\delta(\omega_{p'} - \omega_p - \omega_0), \end{aligned} \quad (24)$$

where $\vec{q} = \vec{p}' - \vec{p}$. Note that we have defined $\bar{\phi}(\vec{p})$ as the unnormalised scattered wave function for notational convenience, i.e. $\bar{\phi}(\vec{p}) = \sqrt{P_{e \rightarrow g} \phi_{\text{scatt}}(\vec{p})}$. We also note that only momenta \vec{q} with $|\vec{q}|$ close to $\hbar\omega_0/c$ contribute significantly to the integral. Since $\omega_p = c\sqrt{|\vec{p}|^2 + m^2 c^2} / \hbar \gg \omega_0$, the energy conservation implies that

$$|\vec{p}|^2 = (\hbar\omega_p/c)^2 - m^2 c^2 = (\hbar(\omega_{p'} - \omega_0)/c)^2 - m^2 c^2 \approx |\vec{p}'|^2 - \frac{2\hbar^2 \omega_{p'} \omega_0}{c^2}. \quad (25)$$

Then,

$$\frac{2\hbar^2\omega_{p'}\omega_0}{c^2} \approx |\vec{p}'|^2 - |\vec{p}|^2 = |\vec{p}'|^2 - |\vec{p}' - \vec{q}|^2 = 2\vec{q} \cdot \vec{p}' - |\vec{q}|^2. \quad (26)$$

We define $\zeta(\vec{q}) := \vec{q} \cdot \vec{p}' - \frac{|\vec{q}|^2}{2}$ and find

$$\delta(\omega_{p'} - \omega_p - \omega_0) = \left| \frac{\partial \omega_p}{\partial \zeta} \right|^{-1} \delta \left(\zeta(\vec{q}) - \frac{\hbar^2 \omega_0 \omega_{p'}}{c^2} \right) = \frac{\hbar^2 \omega_p}{c^2} \delta \left(\zeta(\vec{q}) - \frac{\hbar^2 \omega_0 \omega_{p'}}{c^2} \right). \quad (27)$$

Energy conservation also implies

$$\frac{\sqrt{\omega_p}}{\sqrt{\omega_{p'}}} = \frac{\sqrt{\omega_{p'} - \omega_0}}{\sqrt{\omega_{p'}}} \approx \left(1 - \frac{\omega_0}{2\omega_{p'}} \right) \approx 1. \quad (28)$$

Thus,

$$\bar{\phi}(\vec{p}') = -e\mu_0 \hbar p'_j \int \frac{d^3 q}{(2\pi\hbar)^3} \phi_{\text{in}}(\vec{p}' - \vec{q}) \epsilon^{jkl} \mu_k q_l \lim_{\epsilon \rightarrow 0^+} \left[\frac{1}{(\hbar\omega_0/c)^2 - |\vec{q}|^2 + i\epsilon} \right] 2\pi \delta \left(\zeta(\vec{q}) - \frac{\hbar^2 \omega_0 \omega_{p'}}{c^2} \right). \quad (29)$$

We consider an initial state that factorizes into a transversal Gaussian distribution with width Δp_\perp and longitudinal distribution that we specify later, that is

$$\phi_{\text{in}}(\vec{p}) = \phi_{\text{in},z}(p_z) \phi_{\text{in},\perp}(\vec{p}_\perp), \quad (30)$$

where we decomposed $\vec{p} = \vec{p}_z + \vec{p}_\perp$, where \vec{p}_z and \vec{p}_\perp are parallel and perpendicular to the z -axis, respectively. We assume that the initial state of the beam in real space is a Gaussian wave packet displaced by $\vec{r}_{0,\perp}$, that is

$$\psi_{\text{in},\perp}^e(\vec{r}_\perp, t) = \tilde{\psi}_{\text{in},\perp}^e(\vec{r}_\perp - \vec{r}_{0,\perp}, t) \quad (31)$$

and $\tilde{\psi}_{\text{in},\perp}^e$ reaches its minimal extension at t_0 . In momentum space, this displacement leads to a factor $e^{-i\vec{p}_\perp \cdot \vec{r}_{0,\perp}/\hbar}$, and we find the normalized Gaussian

$$\phi_{\text{in},\perp}(\vec{p}_\perp) = \frac{\sqrt{2\pi\hbar}}{\Delta p_\perp} e^{-i\vec{p}_\perp \cdot \vec{r}_{0,\perp}/\hbar} e^{-\frac{(\vec{p}_\perp)^2}{4\Delta p_\perp^2}}. \quad (32)$$

We obtain

$$\begin{aligned} \bar{\phi}(\vec{p}') &= -e\mu_0 \hbar p'_j \int \frac{d^3 q}{(2\pi\hbar)^3} \phi_{\text{in},z}(p'_z - q_z) \frac{\sqrt{2\pi\hbar}}{\Delta p_\perp} e^{-i(\vec{p}'_\perp - \vec{q}_\perp) \cdot \vec{r}_{0,\perp}/\hbar} e^{-\frac{(\vec{p}'_\perp - \vec{q}_\perp)^2}{4\Delta p_\perp^2}} \\ &\quad \epsilon^{jkl} \mu_k q_l \lim_{\epsilon \rightarrow 0^+} \left[\frac{1}{(\hbar\omega_0/c)^2 - |\vec{q}|^2 + i\epsilon} \right] 2\pi \delta \left(\zeta(\vec{q}) - \frac{\hbar^2 \omega_0 \omega_{p'}}{c^2} \right). \end{aligned} \quad (33)$$

As we consider fast electrons, the initial wave function will be strongly peaked for momenta with $p_z \gg |\vec{p}_\perp|$, that is the expectation value of p_z with respect to $\phi_{\text{in},z}(p_z)$ is $p_{z,0} \gg |\vec{p}_\perp|$ and $p_{z,0} \gg \Delta p_z$, where $(\Delta p_z)^2$ is the variance of p_z . The same will be true for the final momentum wave function. Therefore, we approximate

$$\zeta(\vec{q}) - \frac{\hbar^2 \omega_0 \omega_{p'}}{c^2} \approx q_z p'_z - \frac{\hbar^2 \omega_0 \omega_{p'}^z}{c^2} \quad (34)$$

where $\omega_{p'}^z = c\sqrt{|p'_z|^2 + m^2 c^2}/\hbar$ and

$$\begin{aligned} \bar{\phi}(\vec{p}') &\approx -e\mu_0 \hbar p'_j \int \frac{d^3 q}{(2\pi\hbar)^3} \phi_{\text{in},z}(p'_z - q_z) \frac{\sqrt{2\pi\hbar}}{\Delta p_\perp} e^{-i(\vec{p}'_\perp - \vec{q}_\perp) \cdot \vec{r}_{0,\perp}/\hbar} e^{-\frac{(\vec{p}'_\perp - \vec{q}_\perp)^2}{4\Delta p_\perp^2}} \\ &\quad \epsilon^{jkl} \mu_k q_l \lim_{\epsilon \rightarrow 0^+} \left[\frac{1}{(\hbar\omega_0/c)^2 - |\vec{q}|^2 + i\epsilon} \right] 2\pi \frac{1}{p'_z} \delta \left(q_z - \frac{\hbar^2 \omega_0 \omega_{p'}^z}{c^2 p'_z} \right) \\ &= e\mu_0 \phi_{\text{in},z}(p'_z - \delta p'_z(p'_z)) \int \frac{d^2 q_\perp}{(2\pi\hbar)^2} \frac{\sqrt{2\pi\hbar}}{\Delta p_\perp} e^{-\frac{i}{\hbar}(\vec{p}'_\perp - \vec{q}_\perp) \cdot \vec{r}_{0,\perp}} e^{-\frac{(\vec{p}'_\perp - \vec{q}_\perp)^2}{4\Delta p_\perp^2}} \frac{\epsilon^{zkl} \mu_k \left(q_{\perp,l} - \frac{\delta p'_z}{p'_z} p'_{\perp,l} \right)}{a(p'_z)^2 + |\vec{q}_\perp|^2}, \end{aligned} \quad (35)$$

where we have performed the trivial limit of $\epsilon \rightarrow 0^+$ and we defined

$$\delta p'_z(p'_z) = \frac{\hbar^2 \omega_0 \omega_{p'_z}^z}{c^2 p'_z} = \frac{\hbar \omega_0}{v'_z} \quad (36)$$

and

$$a(p'_z) = \sqrt{(\hbar \omega_0 / c)^2 ((\hbar \omega_{p'_z}^z / c p'_z)^2 - 1)} = \frac{\hbar \omega_0}{\gamma' v'_z}. \quad (37)$$

We find that the scattered momentum wave function is shifted in the p_z -direction by $\delta p'_z(p'_z)$ and deflected in the perpendicular directions. In the following, we will not display the dependence of a and $\delta p'_z$ on p'_z in most equations for the sake of readability.

The overlap integral

We find for the overlap integral

$$\begin{aligned} \langle \text{el} | \text{in} | \text{out} \rangle_{\text{el}} &= (P_{e \rightarrow g})^{-1/2} \int \frac{d^3 p'}{(2\pi\hbar)^3} \phi_{\text{in}}^*(\vec{p}') \bar{\phi}(\vec{p}') \\ &= e\mu_0 (P_{e \rightarrow g})^{-1/2} \int \frac{dp'_z}{2\pi\hbar} \phi_{\text{in},z}^*(p'_z) \phi_{\text{in},z}(p'_z - \delta p'_z) \int \frac{d^2 p'_\perp}{2\pi(\Delta p_\perp)^2} \int \frac{d^2 q_\perp}{(2\pi\hbar)^2} \\ &\quad e^{i\vec{p}'_\perp \cdot \vec{r}_{0,\perp} / \hbar} e^{-\frac{(\vec{p}'_\perp)^2}{4\Delta p_\perp^2}} e^{-\frac{i}{\hbar}(\vec{p}'_\perp - \vec{q}_\perp) \cdot \vec{r}_{0,\perp}} e^{-\frac{(\vec{p}'_\perp - \vec{q}_\perp)^2}{4\Delta p_\perp^2}} \frac{\epsilon^{zkl} \mu_k \left(q_{\perp,l} - \frac{\delta p'_z}{p'_z} p'_{\perp,l} \right)}{a^2 + |\vec{q}_\perp|^2} \\ &= e\mu_0 (P_{e \rightarrow g})^{-1/2} \int \frac{dp'_z}{2\pi\hbar} \phi_{\text{in},z}^*(p'_z) \phi_{\text{in},z}(p'_z - \delta p'_z) \int \frac{d^2 q_\perp}{(2\pi\hbar)^2} e^{\frac{i}{\hbar} \vec{q}_\perp \cdot \vec{r}_{0,\perp}} e^{-\frac{(\vec{q}_\perp)^2}{4\Delta p_\perp^2}} \frac{1}{a^2 + |\vec{q}_\perp|^2} \\ &\quad \int \frac{d^2 p'_\perp}{2\pi(\Delta p_\perp)^2} \epsilon^{zkl} \mu_k \left(q_{\perp,l} - \frac{\delta p'_z}{p'_z} p'_{\perp,l} \right) e^{\frac{\vec{p}'_\perp \cdot \vec{q}_\perp}{2\Delta p_\perp^2}} e^{-\frac{(\vec{p}'_\perp)^2}{2\Delta p_\perp^2}} \\ &= e\mu_0 (P_{e \rightarrow g})^{-1/2} \int \frac{dp'_z}{2\pi\hbar} \phi_{\text{in},z}^*(p'_z) \phi_{\text{in},z}(p'_z - \delta p'_z) \int \frac{d^2 q_\perp}{(2\pi\hbar)^2} e^{\frac{i}{\hbar} \vec{q}_\perp \cdot \vec{r}_{0,\perp}} e^{-\frac{(\vec{q}_\perp)^2}{4\Delta p_\perp^2}} \frac{1}{a^2 + |\vec{q}_\perp|^2} \\ &\quad \epsilon^{zkl} \mu_k \left(q_{\perp,l} - 2\Delta p_\perp^2 \frac{\delta p'_z}{p'_z} \nabla_l^{q_\perp} \right) \int \frac{d^2 p'_\perp}{2\pi(\Delta p_\perp)^2} e^{\frac{\vec{p}'_\perp \cdot \vec{q}_\perp}{2\Delta p_\perp^2}} e^{-\frac{(\vec{p}'_\perp)^2}{2\Delta p_\perp^2}}. \end{aligned} \quad (38)$$

We have

$$\int \frac{d^2 p'_\perp}{2\pi(\Delta p_\perp)^2} e^{\frac{\vec{p}'_\perp \cdot \vec{q}_\perp}{2\Delta p_\perp^2}} e^{-\frac{(\vec{p}'_\perp)^2}{2\Delta p_\perp^2}} = e^{\frac{(\vec{q}_\perp)^2}{8\Delta p_\perp^2}} \int \frac{d^2 p'_\perp}{2\pi(\Delta p_\perp)^2} e^{-\frac{(\vec{q}_\perp/2 - \vec{p}'_\perp)^2}{2\Delta p_\perp^2}} = e^{\frac{(\vec{q}_\perp)^2}{8\Delta p_\perp^2}}. \quad (39)$$

Therefore,

$$\begin{aligned} \langle \text{el} | \text{in} | \text{out} \rangle_{\text{el}} &= e\mu_0 (P_{e \rightarrow g})^{-1/2} \int \frac{dp'_z}{2\pi\hbar} \phi_{\text{in},z}^*(p'_z) \phi_{\text{in},z}(p'_z - \delta p'_z) \epsilon^{zkl} \mu_k \left(1 - \frac{1}{2} \frac{\delta p'_z}{p'_z} \right) \\ &\quad \int \frac{d^2 q_\perp}{(2\pi\hbar)^2} e^{\frac{i}{\hbar} \vec{q}_\perp \cdot \vec{r}_{0,\perp}} e^{-\frac{(\vec{q}_\perp)^2}{8\Delta p_\perp^2}} \frac{q_{\perp,l}}{a^2 + |\vec{q}_\perp|^2}. \end{aligned}$$

The last integral can be rewritten as

$$\int \frac{d^2 q_\perp}{(2\pi\hbar)^2} e^{\frac{i}{\hbar} \vec{q}_\perp \cdot \vec{r}_{0,\perp}} e^{-\frac{(\vec{q}_\perp)^2}{8\Delta p_\perp^2}} \frac{q_{\perp,l}}{a + |\vec{q}_\perp|^2} = \frac{\hbar}{i} \nabla_l^{r_{0,\perp}} \int \frac{d^2 q_\perp}{(2\pi\hbar)^2} e^{\frac{i}{\hbar} \vec{q}_\perp \cdot \vec{r}_{0,\perp}} e^{-\frac{(\vec{q}_\perp)^2}{8\Delta p_\perp^2}} \frac{1}{a^2 + |\vec{q}_\perp|^2}. \quad (40)$$

We use that

$$\frac{1}{a^2 + |\vec{q}_\perp|^2} = \frac{1}{4\pi\hbar^2} \int d^3 r \frac{e^{-\frac{i}{\hbar} a z} e^{-\frac{i}{\hbar} \vec{q}_\perp \cdot \vec{r}_\perp}}{\sqrt{z^2 + |\vec{r}_\perp|^2}} = \frac{1}{2\pi\hbar^2} \int d^2 r_\perp K_0(a|\vec{r}_\perp|/\hbar) e^{-\frac{i}{\hbar} \vec{q}_\perp \cdot \vec{r}_\perp} \quad (41)$$

and find

$$\begin{aligned}
& \frac{\hbar}{i} \nabla_l^{r_{0,\perp}} \int \frac{d^2 q_\perp}{(2\pi\hbar)^2} e^{\frac{i}{\hbar} \vec{q}_\perp \cdot \vec{r}_{0,\perp}} e^{-\frac{(\vec{q}_\perp)^2}{8\Delta p_\perp^2}} \frac{1}{a^2 + |\vec{q}_\perp|^2} \\
&= -i \frac{1}{2\pi\hbar} \nabla_l^{r_{0,\perp}} \int \frac{d^2 q_\perp}{(2\pi\hbar)^2} e^{\frac{i}{\hbar} \vec{q}_\perp \cdot \vec{r}_{0,\perp}} e^{-\frac{(\vec{q}_\perp)^2}{8\Delta p_\perp^2}} \int d^2 r_\perp K_0(a|\vec{r}_\perp|/\hbar) e^{-\frac{i}{\hbar} \vec{q}_\perp \cdot \vec{r}_\perp} \\
&= -i \frac{1}{2\pi\hbar} \nabla_l^{r_{0,\perp}} \int d^2 r_\perp K_0(a|\vec{r}_\perp|/\hbar) \int \frac{d^2 q_\perp}{(2\pi\hbar)^2} e^{-\frac{i}{\hbar} \vec{q}_\perp \cdot (\vec{r}_\perp - \vec{r}_{0,\perp})} e^{-\frac{(\vec{q}_\perp)^2}{8\Delta p_\perp^2}} \\
&= -i \frac{1}{2\pi\hbar} \nabla_l^{r_{0,\perp}} \int d^2 r_\perp K_0(a|\vec{r}_\perp|/\hbar) \frac{2\Delta p_\perp^2}{\pi\hbar^2} e^{-\frac{2\Delta p_\perp^2 (\vec{r}_\perp - \vec{r}_{0,\perp})^2}{\hbar^2}} \\
&= -i \frac{1}{2\pi\hbar} \nabla_l^{r_{0,\perp}} \int \frac{d^2 r_\perp}{2\pi\Delta r_\perp^2} K_0(a|\vec{r}_\perp|/\hbar) e^{-\frac{(\vec{r}_\perp - \vec{r}_{0,\perp})^2}{2\Delta r_\perp^2}}, \tag{42}
\end{aligned}$$

where $\Delta r_\perp = \hbar/(2\Delta p_\perp)$. Since $K_0(a|\vec{r}_\perp|/\hbar) = \int dz e^{-\frac{i}{\hbar} az} (z^2 + |\vec{r}_\perp|^2)^{-1/2}$, we recover the effect of the magnetic field due to a magnetic dipole on a Gaussian electron wave packet. If the wave packet is well localised with respect to $K_0(a|\vec{r}_\perp|/\hbar)$ at $|\vec{r}_{0,\perp}|$, then we can approximate the integral over \vec{r}_\perp by replacing it with the value of the integrand at $\vec{r}_{0,\perp}$. More concretely, given that $a(p'_z)\Delta r_\perp/\hbar = \omega_0\Delta r_\perp/(\gamma'_z v'_z) \ll 1$ for all momenta p'_z in a range Δp_z around the peak value $p_{z,0}$ and $|r_{0,\perp}|/\Delta r_\perp \gg 1$ for all considerations in this article,

$$-i \frac{1}{2\pi\hbar} \nabla_l^{r_{0,\perp}} \int \frac{d^2 r_\perp}{2\pi\Delta r_\perp^2} K_0(a|\vec{r}_\perp|/\hbar) e^{-\frac{(\vec{r}_\perp - \vec{r}_{0,\perp})^2}{2\Delta r_\perp^2}} \approx i \frac{a}{2\pi\hbar^2} \frac{(\vec{r}_{0,\perp})_l}{|\vec{r}_{0,\perp}|} K_1(a|\vec{r}_{0,\perp}|/\hbar) \tag{43}$$

For all momenta p'_z in a range Δp_z around the peak value $p_{z,0}$, we also have $a(p'_z)|\vec{r}_{0,\perp}|/\hbar = \omega_0|\vec{r}_{0,\perp}|/(\gamma'_z v'_z) \ll 1$ for all considerations in this article. Therefore,

$$i \frac{a}{2\pi\hbar^2} \frac{(\vec{r}_{0,\perp})_l}{|\vec{r}_{0,\perp}|} K_1(a|\vec{r}_{0,\perp}|/\hbar) \approx i \frac{1}{2\pi\hbar} \frac{(\vec{r}_{0,\perp})_l}{|\vec{r}_{0,\perp}|^2}, \tag{44}$$

and for the overlap integral,

$$\langle \text{el} | \text{in} | \text{out} \rangle_{\text{el}} \approx i \frac{e\mu_0}{2\pi\hbar} (P_{e \rightarrow g})^{-1/2} \epsilon^{zkl} \mu_k \frac{(\vec{r}_{0,\perp})_l}{|\vec{r}_{0,\perp}|^2} \int \frac{dp'_z}{2\pi\hbar} \phi_{\text{in},z}^*(p'_z) \phi_{\text{in},z}(p'_z - \delta p'_z(p'_z)) \left(1 - \frac{1}{2} \frac{\delta p'_z(p'_z)}{p'_z} \right). \tag{45}$$

Above, we restricted our considerations to the situation of longitudinal wave functions with an expectation value $p_{z,0} \gg |\vec{p}_\perp|$ and $p_{z,0} \gg \Delta p_z$, where $(\Delta p_z)^2$ is the variance of p_z . This implies that we can make the replacement $\delta p'_z(p'_z) \rightarrow \delta p'_z(p_{z,0})$ in the above integral and approximate

$$\langle \text{el} | \text{in} | \text{out} \rangle_{\text{el}} \approx i \frac{e\mu_0}{2\pi\hbar} (P_{e \rightarrow g})^{-1/2} \epsilon^{zkl} \mu_k \frac{(\vec{r}_{0,\perp})_l}{|\vec{r}_{0,\perp}|^2} \int \frac{dp'_z}{2\pi\hbar} \phi_{\text{in},z}^*(p'_z) \phi_{\text{in},z}(p'_z - \delta p'_z(p_{z,0})). \tag{46}$$

The transition probability

In the next step, we calculate the transition probability

$$\begin{aligned}
P_{e \rightarrow g} &= \int \frac{d^3 p'}{(2\pi\hbar)^3} \bar{\phi}^*(\vec{p}') \bar{\phi}(\vec{p}') \\
&= (\epsilon\mu_0)^2 \int \frac{dp'_z}{2\pi\hbar} \phi_{\text{in},z}^*(p'_z - \delta p'_z) \phi_{\text{in},z}(p'_z - \delta p'_z) \\
&\quad \int \frac{d^2 p'_\perp}{2\pi\Delta p_\perp^2} \left| \int \frac{d^2 q_\perp}{(2\pi\hbar)^2} e^{\frac{i}{\hbar} \vec{q}_\perp \cdot \vec{r}_{0,\perp}} e^{-\frac{(\vec{p}'_\perp - \vec{q}_\perp)^2}{4\Delta p_\perp^2}} \frac{\epsilon^{zkl} \mu_k \left(q_{\perp,l} - \frac{\delta p'_z}{p'_z} p'_{\perp,l} \right)}{a^2 + |\vec{q}_\perp|^2} \right|^2. \tag{47}
\end{aligned}$$

We obtain

$$\begin{aligned}
& \int \frac{d^2 q_\perp}{(2\pi\hbar)^2} e^{\frac{i}{\hbar} \vec{q}_\perp \cdot \vec{r}_{0,\perp}} e^{-\frac{(\vec{p}'_\perp - \vec{q}_\perp)^2}{4\Delta p_\perp^2}} \frac{\epsilon^{zkl} \mu_k \left(q_{\perp,l} - \frac{\delta p'_z}{p'_z} p'_{\perp,l} \right)}{a^2 + |\vec{q}_\perp|^2} \\
&= \int \frac{d^2 q_\perp}{(2\pi\hbar)^2} e^{-\frac{|\vec{p}'_\perp|^2}{4\Delta p_\perp^2}} e^{\frac{i}{\hbar} \vec{q}_\perp \cdot \vec{r}_{0,\perp}} \frac{e^{-\frac{|\vec{q}_\perp|^2}{4\Delta p_\perp^2}}}{a^2 + |\vec{q}_\perp|^2} \epsilon^{zkl} \mu_k \left(q_{\perp,l} - 2\Delta p_\perp^2 \frac{\delta p'_z}{p'_z} \nabla_l^{q_\perp} \right) e^{\frac{\vec{p}'_\perp \cdot \vec{q}_\perp}{2\Delta p_\perp^2}} \tag{48}
\end{aligned}$$

and

$$\begin{aligned}
I_1 &:= \int \frac{d^2 p'_\perp}{2\pi\Delta p_\perp^2} \left| \int \frac{d^2 q_\perp}{(2\pi\hbar)^2} e^{\frac{i}{\hbar}\vec{q}_\perp \cdot \vec{r}_{0,\perp}} e^{-\frac{(\vec{p}'_\perp - \vec{q}_\perp)^2}{4\Delta p_\perp^2}} \frac{\epsilon^{zkl} \mu_k \left(q_{\perp,l} - \frac{\delta p'_z}{p'_z} p'_{\perp,l} \right)}{a^2 + |\vec{q}_\perp|^2} \right|^2 \\
&= \int \frac{d^2 q'_\perp}{(2\pi\hbar)^2} \int \frac{d^2 q_\perp}{(2\pi\hbar)^2} e^{-\frac{i}{\hbar}(\vec{q}'_\perp - \vec{q}_\perp) \cdot \vec{r}_{0,\perp}} \frac{e^{-\frac{|\vec{q}'_\perp|^2}{4\Delta p_\perp^2}}}{a^2 + |\vec{q}'_\perp|^2} \frac{e^{-\frac{|\vec{q}_\perp|^2}{4\Delta p_\perp^2}}}{a^2 + |\vec{q}_\perp|^2} \\
&\quad \epsilon^{zk'l'} \mu_{k'} \left(p'_z q'_{\perp,l'} - 2\Delta p_\perp^2 \delta p'_z \nabla_{l'}^{q'_\perp} \right) \epsilon^{zkl} \mu_k \left(q_{\perp,l} - 2\Delta p_\perp^2 \frac{\delta p'_z}{p'_z} \nabla_l^{q_\perp} \right) \int \frac{d^2 p'_\perp}{2\pi\Delta p_\perp^2} e^{-\frac{|\vec{p}'_\perp|^2}{2\Delta p_\perp^2}} e^{\frac{\vec{p}'_\perp \cdot (\vec{q}'_\perp + \vec{q}_\perp)}{2\Delta p_\perp^2}}.
\end{aligned} \tag{49}$$

We integrate the Gaussian

$$\int \frac{d^2 p'_\perp}{2\pi\Delta p_\perp^2} e^{-\frac{|\vec{p}'_\perp|^2}{2\Delta p_\perp^2}} e^{\frac{\vec{p}'_\perp \cdot (\vec{q}'_\perp + \vec{q}_\perp)}{2\Delta p_\perp^2}} = e^{\frac{|\vec{q}'_\perp + \vec{q}_\perp|^2}{8\Delta p_\perp^2}} \int \frac{d^2 p'_\perp}{2\pi\Delta p_\perp^2} e^{-\frac{|\vec{p}'_\perp - (\vec{q}'_\perp + \vec{q}_\perp)/2|^2}{2\Delta p_\perp^2}} = e^{\frac{|\vec{q}'_\perp + \vec{q}_\perp|^2}{8\Delta p_\perp^2}} \tag{50}$$

such that after taking the derivatives for q'_\perp and q_\perp ,

$$\begin{aligned}
I_1 &= \int \frac{d^2 q'_\perp}{(2\pi\hbar)^2} \int \frac{d^2 q_\perp}{(2\pi\hbar)^2} e^{-\frac{i}{\hbar}(\vec{q}'_\perp - \vec{q}_\perp) \cdot \vec{r}_{0,\perp}} \frac{e^{-\frac{|\vec{q}'_\perp|^2}{4\Delta p_\perp^2}}}{a^2 + |\vec{q}'_\perp|^2} \frac{e^{-\frac{|\vec{q}_\perp|^2}{4\Delta p_\perp^2}}}{a^2 + |\vec{q}_\perp|^2} \\
&\quad \epsilon^{zk'l'} \mu_{k'} \left(q'_{\perp,l'} - \frac{1}{2} \frac{\delta p'_z}{p'_z} (q'_{\perp,l'} + q_{\perp,l'}) \right) \epsilon^{zkl} \mu_k \left(q_{\perp,l} - \frac{1}{2} \frac{\delta p'_z}{p'_z} (q_{\perp,l} + q_{\perp,l}) \right) e^{\frac{|\vec{q}'_\perp + \vec{q}_\perp|^2}{8\Delta p_\perp^2}} \\
&= \int \frac{d^2 q'_\perp}{(2\pi\hbar)^2} \int \frac{d^2 q_\perp}{(2\pi\hbar)^2} e^{-\frac{i}{\hbar}(\vec{q}'_\perp - \vec{q}_\perp) \cdot \vec{r}_{0,\perp}} e^{-\frac{|\vec{q}'_\perp - \vec{q}_\perp|^2}{8\Delta p_\perp^2}} \frac{1}{a^2 + |\vec{q}'_\perp|^2} \frac{1}{a^2 + |\vec{q}_\perp|^2} \\
&\quad \epsilon^{zk'l'} \mu_{k'} \left(q'_{\perp,l'} - \frac{1}{2} \frac{\delta p'_z}{p'_z} (q'_{\perp,l'} + q_{\perp,l'}) \right) \epsilon^{zkl} \mu_k \left(q_{\perp,l} - \frac{1}{2} \frac{\delta p'_z}{p'_z} (q_{\perp,l} + q_{\perp,l}) \right).
\end{aligned} \tag{51}$$

We use the Fourier transforms

$$\frac{1}{a^2 + |\vec{q}_\perp|^2} = \frac{1}{4\pi\hbar^2} \int d^3 r \frac{e^{-\frac{i}{\hbar}az} e^{-\frac{i}{\hbar}\vec{q}_\perp \cdot \vec{r}_\perp}}{\sqrt{z^2 + |\vec{r}_\perp|^2}} = \frac{1}{2\pi\hbar^2} \int d^2 r_\perp K_0(a|\vec{r}_\perp|/\hbar) e^{-\frac{i}{\hbar}\vec{q}_\perp \cdot \vec{r}_\perp} \tag{52}$$

$$e^{-\frac{|\vec{q}'_\perp - \vec{q}_\perp|^2}{8\Delta p_\perp^2}} = \frac{2\Delta p_\perp^2}{\pi\hbar^2} \int d^2 r_\perp e^{-\frac{i}{\hbar}(\vec{q}'_\perp - \vec{q}_\perp) \cdot \vec{r}_\perp} e^{-\frac{2\Delta p_\perp^2 |\vec{r}_\perp|^2}{\hbar^2}} = \frac{1}{2\pi\Delta r_\perp^2} \int d^2 r_\perp e^{-\frac{i}{\hbar}(\vec{q}'_\perp - \vec{q}_\perp) \cdot \vec{r}_\perp} e^{-\frac{|\vec{r}_\perp|^2}{2\Delta r_\perp^2}}, \tag{53}$$

to obtain

$$\begin{aligned}
I_1 &= \frac{1}{2\pi\hbar^2} \int d^2 r_\perp K_0(a|\vec{r}_\perp|/\hbar) \frac{1}{2\pi\hbar^2} \int d^2 r'_\perp K_0(a|\vec{r}'_\perp|/\hbar) \frac{1}{2\pi\Delta r_\perp^2} \int d^2 r''_\perp e^{-\frac{|\vec{r}''_\perp|^2}{2\Delta r_\perp^2}} \\
&\quad \int \frac{d^2 q'_\perp}{(2\pi\hbar)^2} \int \frac{d^2 q_\perp}{(2\pi\hbar)^2} e^{-\frac{i}{\hbar}(\vec{q}'_\perp - \vec{q}_\perp) \cdot (\vec{r}_{0,\perp} + \vec{r}'_\perp)} e^{-\frac{i}{\hbar}\vec{q}'_\perp \cdot \vec{r}'_\perp} e^{-\frac{i}{\hbar}\vec{q}_\perp \cdot \vec{r}_\perp} \\
&\quad \epsilon^{zk'l'} \mu_{k'} \left(q'_{\perp,l'} - \frac{1}{2} \frac{\delta p'_z}{p'_z} (q'_{\perp,l'} + q_{\perp,l'}) \right) \epsilon^{zkl} \mu_k \left(q_{\perp,l} - \frac{1}{2} \frac{\delta p'_z}{p'_z} (q_{\perp,l} + q_{\perp,l}) \right) \\
&= -\frac{1}{(2\pi\hbar)^2} \int d^2 r_\perp K_0(a|\vec{r}_\perp|/\hbar) \int d^2 r'_\perp K_0(a|\vec{r}'_\perp|/\hbar) \frac{1}{2\pi\Delta r_\perp^2} \int d^2 r''_\perp e^{-\frac{|\vec{r}''_\perp|^2}{2\Delta r_\perp^2}} \\
&\quad \epsilon^{zk'l'} \mu_{k'} \left(\nabla_{l'}^{r'_\perp} - \frac{1}{2} \frac{\delta p'_z}{p'_z} (\nabla_{l'}^{r'_\perp} + \nabla_{l'}^{r_\perp}) \right) \epsilon^{zkl} \mu_k \left(\nabla_l^{r_\perp} - \frac{1}{2} \frac{\delta p'_z}{p'_z} (\nabla_l^{r'_\perp} + \nabla_l^{r_\perp}) \right) \\
&\quad \int \frac{d^2 q'_\perp}{(2\pi\hbar)^2} \int \frac{d^2 q_\perp}{(2\pi\hbar)^2} e^{-\frac{i}{\hbar}(\vec{q}'_\perp - \vec{q}_\perp) \cdot (\vec{r}_{0,\perp} + \vec{r}'_\perp)} e^{-\frac{i}{\hbar}\vec{q}'_\perp \cdot \vec{r}'_\perp} e^{-\frac{i}{\hbar}\vec{q}_\perp \cdot \vec{r}_\perp}.
\end{aligned} \tag{54}$$

With partial integration, we find

$$\begin{aligned}
I_1 &= -\frac{1}{(2\pi\hbar)^2} \frac{1}{2\pi\Delta r_\perp^2} \int d^2 r''_\perp e^{-\frac{|\vec{r}''_\perp|^2}{2\Delta r_\perp^2}} \int d^2 r_\perp \int d^2 r'_\perp \delta^{(2)}(\vec{r}'_\perp + \vec{r}_{0,\perp} + \vec{r}''_\perp) \delta^{(2)}(\vec{r}_\perp - (\vec{r}_{0,\perp} + \vec{r}''_\perp)) \\
&\quad \epsilon^{zk'l'} \mu_{k'} \left(\nabla_{l'}^{r'_\perp} - \frac{1}{2} \frac{\delta p'_z}{p'_z} (\nabla_{l'}^{r'_\perp} + \nabla_{l'}^{r_\perp}) \right) \epsilon^{zkl} \mu_k \left(\nabla_l^{r_\perp} - \frac{1}{2} \frac{\delta p'_z}{p'_z} (\nabla_l^{r'_\perp} + \nabla_l^{r_\perp}) \right) K_0 \left(\frac{a|\vec{r}_\perp|}{\hbar} \right) K_0 \left(\frac{a|\vec{r}''_\perp|}{\hbar} \right) \\
&= \frac{1}{(2\pi\hbar)^2} \frac{1}{2\pi\Delta r_\perp^2} \int d^2 r''_\perp e^{-\frac{|\vec{r}''_\perp|^2}{2\Delta r_\perp^2}} \int d^2 r_\perp \int d^2 r'_\perp \delta^{(2)}(\vec{r}'_\perp + \vec{r}_{0,\perp} + \vec{r}''_\perp) \delta^{(2)}(\vec{r}_\perp - (\vec{r}_{0,\perp} + \vec{r}''_\perp)) \\
&\quad \epsilon^{zk'l'} \mu_{k'} \left(\nabla_{l'}^{r'_\perp} - \frac{1}{2} \frac{\delta p'_z}{p'_z} (\nabla_{l'}^{r'_\perp} + \nabla_{l'}^{r_\perp}) \right) \\
&\quad \frac{a}{\hbar} \epsilon^{zkl} \mu_k \left(\left(1 - \frac{1}{2} \frac{\delta p'_z}{p'_z} \right) \frac{r_{\perp,l}}{|\vec{r}_\perp|} K_1 \left(\frac{a|\vec{r}_\perp|}{\hbar} \right) K_0 \left(\frac{a|\vec{r}'_\perp|}{\hbar} \right) - \frac{1}{2} \frac{\delta p'_z}{p'_z} \frac{r'_{\perp,l}}{|\vec{r}'_\perp|} K_0 \left(\frac{a|\vec{r}_\perp|}{\hbar} \right) K_1 \left(\frac{a|\vec{r}'_\perp|}{\hbar} \right) \right) \\
&= -\frac{1}{(2\pi\hbar)^2} \frac{1}{2\pi\Delta r_\perp^2} \int d^2 r''_\perp e^{-\frac{|\vec{r}''_\perp|^2}{2\Delta r_\perp^2}} \int d^2 r_\perp \int d^2 r'_\perp \delta^{(2)}(\vec{r}'_\perp + \vec{r}_{0,\perp} + \vec{r}''_\perp) \delta^{(2)}(\vec{r}_\perp - (\vec{r}_{0,\perp} + \vec{r}''_\perp)) \\
&\quad \frac{a^2}{\hbar^2} \epsilon^{zk'l'} \mu_{k'} \epsilon^{zkl} \mu_k \left(\left(\left(1 - \frac{1}{2} \frac{\delta p'_z}{p'_z} \right)^2 \frac{r_{\perp,l} r'_{\perp,l'}}{|\vec{r}_\perp| |\vec{r}'_\perp|} + \frac{1}{4} \left(\frac{\delta p'_z}{p'_z} \right)^2 \frac{r'_{\perp,l} r_{\perp,l'}}{|\vec{r}'_\perp| |\vec{r}_\perp|} \right) K_1 \left(\frac{a|\vec{r}_\perp|}{\hbar} \right) K_1 \left(\frac{a|\vec{r}'_\perp|}{\hbar} \right) \right. \\
&\quad - \frac{1}{2} \frac{\delta p'_z}{p'_z} \left(1 - \frac{1}{2} \frac{\delta p'_z}{p'_z} \right) \frac{r_{\perp,l} r'_{\perp,l'}}{|\vec{r}_\perp|^2} \left(K_0 \left(\frac{a|\vec{r}_\perp|}{\hbar} \right) + \frac{2\hbar}{a|\vec{r}_\perp|} K_1 \left(\frac{a|\vec{r}_\perp|}{\hbar} \right) \right) K_0 \left(\frac{a|\vec{r}'_\perp|}{\hbar} \right) \\
&\quad - \frac{1}{2} \frac{\delta p'_z}{p'_z} \left(1 - \frac{1}{2} \frac{\delta p'_z}{p'_z} \right) \frac{r'_{\perp,l} r_{\perp,l'}}{|\vec{r}'_\perp|^2} K_0 \left(\frac{a|\vec{r}_\perp|}{\hbar} \right) \left(K_0 \left(\frac{a|\vec{r}'_\perp|}{\hbar} \right) + \frac{2\hbar}{a|\vec{r}'_\perp|} K_1 \left(\frac{a|\vec{r}'_\perp|}{\hbar} \right) \right) \\
&\quad \left. + \frac{1}{2} \frac{\delta p'_z}{p'_z} \left(1 - \frac{1}{2} \frac{\delta p'_z}{p'_z} \right) \delta_{l,l'} \left(\frac{\hbar}{a|\vec{r}_\perp|} K_1 \left(\frac{a|\vec{r}_\perp|}{\hbar} \right) K_0 \left(\frac{a|\vec{r}'_\perp|}{\hbar} \right) + \frac{\hbar}{a|\vec{r}'_\perp|} K_0 \left(\frac{a|\vec{r}_\perp|}{\hbar} \right) K_1 \left(\frac{a|\vec{r}'_\perp|}{\hbar} \right) \right) \right).
\end{aligned} \tag{55}$$

Taking into account that $a(p'_z)\Delta r_\perp/\hbar \ll 1$ for all momenta p'_z in a range Δp_z around the peak value $p_{z,0}$ and that $|r_{0,\perp}|/\Delta r_\perp \gg 1$ for all considerations in this article, we approximate the integration over \vec{r}''_\perp by evaluating the integrand at $\vec{r}''_\perp = 0$ and we find

$$\begin{aligned}
I_1 &\approx \frac{a^2}{(2\pi\hbar^2)^2} \epsilon^{zk'l'} \mu_{k'} \epsilon^{zkl} \mu_k \left(\frac{r_{0,\perp,l} r_{0,\perp,l'}}{|\vec{r}_{0,\perp}|^2} \left(\left(1 - \frac{1}{2} \frac{\delta p'_z}{p'_z} \right)^2 + \frac{1}{4} \left(\frac{\delta p'_z}{p'_z} \right)^2 \right) K_1 \left(\frac{a|\vec{r}_{0,\perp}|}{\hbar} \right)^2 \right. \\
&\quad + \frac{\delta p'_z}{p'_z} \left(1 - \frac{1}{2} \frac{\delta p'_z}{p'_z} \right) \frac{r_{0,\perp,l} r_{0,\perp,l'}}{|\vec{r}_{0,\perp}|^2} K_0 \left(\frac{a|\vec{r}_{0,\perp}|}{\hbar} \right) \left(K_0 \left(\frac{a|\vec{r}_{0,\perp}|}{\hbar} \right) + \frac{2\hbar}{a|\vec{r}_{0,\perp}|} K_1 \left(\frac{a|\vec{r}_{0,\perp}|}{\hbar} \right) \right) \\
&\quad \left. - \frac{\delta p'_z}{p'_z} \left(1 - \frac{1}{2} \frac{\delta p'_z}{p'_z} \right) \delta_{l,l'} \frac{\hbar}{a|\vec{r}_{0,\perp}|} K_0 \left(\frac{a|\vec{r}_{0,\perp}|}{\hbar} \right) K_1 \left(\frac{a|\vec{r}_{0,\perp}|}{\hbar} \right) \right).
\end{aligned} \tag{56}$$

Taking also into account that $a(p'_z)|\vec{r}_{0,\perp}|/\hbar \ll 1$ for all momenta p'_z in a range Δp_z around the peak value $p_{z,0}$, and $p'_z \gg \delta p'_z$, we obtain

$$I_1 \approx \frac{1}{(2\pi\hbar)^2} \epsilon^{zk'l'} \mu_{k'} \epsilon^{zkl} \mu_k \frac{r_{0,\perp,l} r_{0,\perp,l'}}{|\vec{r}_{0,\perp}|^4} = \left(\frac{1}{2\pi\hbar} \epsilon^{zkl} \mu_k \frac{r_{0,\perp,l}}{|\vec{r}_{0,\perp}|^2} \right)^2. \tag{57}$$

We find for the transition probability

$$\begin{aligned}
P_{e \rightarrow g} &= \int \frac{d^3 p'}{(2\pi\hbar)^3} \bar{\phi}^*(\vec{p}') \bar{\phi}(\vec{p}') \\
&= \left(\frac{e\mu_0}{2\pi\hbar} \epsilon^{zkl} \mu_k \frac{r_{0,\perp,l}}{|\vec{r}_{0,\perp}|^2} \right)^2 \int \frac{dp'_z}{2\pi\hbar} \phi_{\text{in},z}^*(p'_z - \delta p'_z) \phi_{\text{in},z}(p'_z - \delta p'_z) \\
&= \left(\frac{e\mu_0}{2\pi\hbar} \epsilon^{zkl} \mu_k \frac{r_{0,\perp,l}}{|\vec{r}_{0,\perp}|^2} \right)^2,
\end{aligned} \tag{58}$$

where we used the normalization of $\phi_{\text{in},z}$.

This result can be compared with the transition probability for a single classical point-like electron passing the quantum system. We start from the interaction Hamiltonian $H_{\text{int}} = -\hat{\mu} \cdot \vec{B}$ to obtain the out-state to first order

$$|\text{out}\rangle_{\text{qs}} \approx \left(\mathbb{I} + \frac{i}{\hbar} \int_{-\infty}^{\infty} dt \hat{\mu} \cdot \vec{B} \right) |e\rangle. \quad (59)$$

For the transition probability, we find

$$P_{e \rightarrow g} = \frac{1}{\hbar^2} \left| \langle g | \int_{-\infty}^{\infty} dt \hat{\mu} \cdot \vec{B} | e \rangle \right|^2 = \frac{1}{\hbar^2} \left| \int_{-\infty}^{\infty} dt \vec{\mu} \cdot \vec{B} \right|^2. \quad (60)$$

The magnetic field of the electron moving parallel to the z -axis is

$$\vec{B}_j(0, t) = \frac{\mu_0 e \gamma \vec{v} \times \vec{r}_{0,\perp}}{4\pi (|\vec{r}_{0,\perp}|^2 + \gamma^2 v^2 (t - t_j)^2)^{3/2}} \quad (61)$$

where $\vec{r}_{0,\perp} = (x_0, y_0, 0)$ and $\vec{v} = (0, 0, v)$. Then,

$$\int_{-\infty}^{\infty} dt \vec{\mu} \cdot \vec{B} = \frac{\mu_0 e}{4\pi} \epsilon^{zjk} \mu_k r_{0,\perp,j} \int_{-\infty}^{\infty} d(\gamma vt) \frac{1}{(|\vec{r}_{0,\perp}|^2 + (\gamma vt)^2)^{3/2}} = \frac{\mu_0 e}{2\pi} \epsilon^{zjk} \mu_k \frac{r_{0,\perp,j}}{|\vec{r}_{0,\perp}|^2}, \quad (62)$$

and

$$P_{e \rightarrow g} = \left(\frac{e \mu_0}{2\pi \hbar} \epsilon^{zkl} \mu_k \frac{r_{0,\perp,l}}{|\vec{r}_{0,\perp}|^2} \right)^2, \quad (63)$$

which coincides with the above approximate result of QED.

The normalized overlap

We combine the transition probability with the overlap integral and find

$${}_{\text{el}}\langle \text{in} | \text{out} \rangle_{\text{el}} \approx i \int \frac{dp_z}{2\pi \hbar} \phi_{\text{in},z}^*(p_z) \phi_{\text{in},z}(p_z - \delta p_z). \quad (64)$$

We consider a Gaussian wave packet

$$\phi_{\text{in},z}(p_z) = \left(\frac{(2\pi)^{1/2} \hbar}{\Delta p_z} \right)^{1/2} e^{-\frac{(p_z - p_{z,0})^2}{4\Delta p_z^2}}. \quad (65)$$

In this case,

$$\begin{aligned} \int \frac{dp_z}{2\pi \hbar} \phi_{\text{in},z}^*(p_z) \phi_{\text{in},z}(p_z - \delta p_z) &= \int \frac{dp_z}{\sqrt{2\pi} \Delta p_z} e^{-\frac{(p_z - p_{z,0})^2 + (p_z - \delta p_z - p_{z,0})^2}{4\Delta p_z^2}} \\ &= e^{-\frac{(\delta p_z)^2}{8\Delta p_z^2}} \int \frac{dp_z}{\sqrt{2\pi} \Delta p_z} e^{-\frac{(p_z - p_{z,0} - \delta p_z/2)^2}{2\Delta p_z^2}} \\ &\approx e^{-\frac{(\delta p_z)^2}{8\Delta p_z^2}}. \end{aligned} \quad (66)$$

Therefore, for the overlap of the in-state and the out-state of the electron, we find

$${}_{\text{el}}\langle \text{in} | \text{out} \rangle_{\text{el}} \approx i e^{-\frac{(\delta p_z)^2}{8\Delta p_z^2}} = i e^{-\frac{\Delta z^2 (\delta p_z)^2}{2\hbar^2}}. \quad (67)$$

We obtain the condition $\delta p_z \ll \hbar/\Delta z$ for the overlap in equation (2) to be close to one. Note that a small size of the electron wave packet is beneficial here. For angular frequencies of the order of 1 GHz and below, and velocities on the order of 10^8 m/s, the condition is fulfilled for $\Delta z \ll v/(2\omega_0) = \lambda_0/(4\pi) \sim 10^{-3}$ m. The size of electron wave packets is defined by the lifetime of electron states in the source which is limited due to phonon-electron and electron-electron scattering [16, 17]. According to the literature on electron microscopy and electron interferometry [7, 18], the size of single electron wave packets is of the order of the coherence length ~ 100 nm. Thus, we conclude that the electron in-state and out-state are nearly indistinguishable and our Condition 1 is fulfilled.

The transversal width of the electron wave packets is bound from above by the focal width $\Delta r_{\perp} < w/2$ of the beam. In this article, we consider distances to the beamline of $d = 5w$. Therefore, we obtain that the condition $|\vec{r}_{0,\perp}|/\Delta r_{\perp} \gg 1$ is indeed fulfilled for almost all of the electrons in the beam. The second condition we used above was $a|\vec{r}_{0,\perp}|/\hbar \ll 1$. The third condition $a\Delta r_{\perp}/\hbar \ll 1$ is then automatically fulfilled. Using the definition of a , we obtain $|\vec{r}_{0,\perp}| \ll \gamma v/\omega_0 = \gamma\lambda_0/(2\pi)$, where λ_0 is the modulation wave length. This condition is always fulfilled in the context of this article.

2. ELECTRON BEAM OF A KLYSTRON

In the following, we will give some details on the current-modulated electron beam in a klystron based on the article [22] by Webster. The electron beam modulation of a klystron is achieved by modulating the kinetic energy, or, effectively, the velocity of electrons in the buncher. This can be done, for example, with a microwave field in a resonator (the buncher cavity) that leads to an electric field in the beam propagation direction [68]. Under the assumption of monochromatic oscillations of the kinetic energy modulation in the buncher and approximating the buncher as infinitesimally short, for the velocity of an electron passing the buncher at time t_1 , we can approximate

$$v = v_0 + v_1 \sin(\omega_0 t_1). \quad (68)$$

When the amplitude of the kinetic energy modulation δE_{kin} is small in comparison to the average kinetic energy, we have $v_1 \approx \delta E_{\text{kin}}/(\gamma^3 m_e v_0)$. The arrival time of the electron at the target (e.g. an atom) is

$$t_2 = t_1 + \frac{l}{v_0 + v_1 \sin(\omega_0 t_1)} \approx t_1 + \frac{l}{v_0} - \frac{lv_1}{v_0^2} \sin(\omega_0 t_1). \quad (69)$$

where l is the distance to the buncher. Charge conservation can be written as $I(t_1, z_1)dt_1 = I(t_2, z_2)dt_2$ and leads to

$$I_2 = \frac{I_1}{1 - r_b \cos(\omega_0 t_1)} = \frac{I_0}{1 - r_b \cos(\omega_0 t_1)} \quad (70)$$

where I_0 is the un-modulated stationary current and

$$r_b = l\omega_0 v_1 / v_0^2 \quad (71)$$

is the bunching parameter. Writing the distance to the buncher as a coordinate $l = z - z_0$, where z_0 is the position

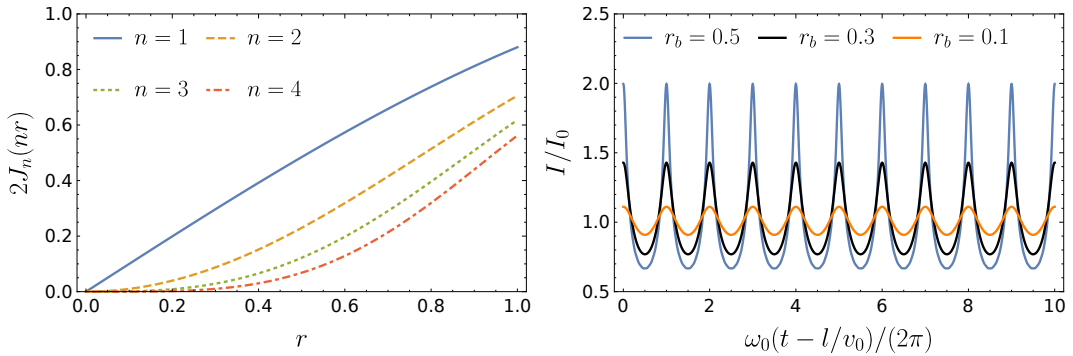


FIG. 4. Left plot: Fourier coefficients of the modulated current for frequencies $n\omega_0$ as a function of the bunching parameter r_b . Right plot: Time dependent current for different bunching parameters.

of the buncher, we obtain

$$I(z, t) = \frac{I_0}{1 - r_b(z) \cos \theta(z, t)} \quad (72)$$

where $\theta(t)$ is the solution of the equation

$$\theta(z, t) - r_b(z) \sin \theta(z, t) = \omega_0 \left(t - \frac{(z - z_0)}{v_0} \right). \quad (73)$$

It has been shown that the current in equation (72) can be expressed as a Fourier series with the coefficients [22]

$$I(z, t) = I_0 \left[1 + \sum_{n=1}^{\infty} 2J_n(n r_b(z)) \cos \left(n\omega_0 \left(t - \frac{(z - z_0)}{v_0} \right) \right) \right], \quad (74)$$

where J_n are the Bessel functions of the first kind. The Fourier coefficients as a function of the bunching parameter are plotted in Fig.4.

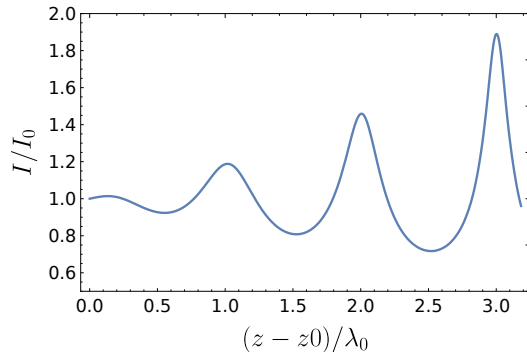


FIG. 5. Spatial change of the electron beam modulation for $v_1/v_2 = 1/40$ at $t = 0$ plotted as a function of the distance from the buncher cavity in units of the modulation wavelength $\lambda_0 = 2\pi v_0/\omega_0$. The spatial range plotted corresponds to the interval $r_b = 0$ to $r_b = 0.5$.

The effect of the electron velocity distribution

The finite width of the electron velocity distribution affects the beam modulation because the bunching of the beam depends on the initial velocity. We consider a kinetic energy distribution with a width ΔE_{kin} of about 1 eV. Approximately, we have $\Delta E_{\text{kin}} = \gamma^3 m v_0 \Delta v_0$. This leads to a distribution in the bunching parameter $\Delta r_b = 2l\omega_0 v_1 \Delta E_{\text{kin}} / (\gamma^3 m v_0^4)$ and $\Delta r_b / r_b = 2\Delta E_{\text{kin}} / (\gamma^3 m v_0^2)$. This ratio decreases for increasing kinetic energies. For $E_{\text{kin}} = 18$ keV, we have $v_0/c \sim 1/4$ and we can find $\Delta r_b / r_b = \Delta E_{\text{kin}} / E_{\text{kin}} \sim 10^{-4}$. We find a minor correction to the bunching parameters which implies a minor correction to the amplitudes of the Fourier components corresponding to the distinct lines in the modulation spectrum. It is also important to note that this effect will not broaden the spectral linewidth of the modulated near field affecting the quantum system.

3. SINGLE PARTICLE BEAM SIMULATION

To analyze systematic effects due to shot noise, we model the electron beam as a collection of single electrons generated in a homogeneous Poisson process. Electrons are generated after waiting times that are exponentially distributed [69] with the mean given by the inverse of the rate σ of electron creation at the cathode. We simulate the beam of a Klystron by modulating the kinetic energy of the particles and propagating them over a drift distance l to obtain the current modulation. The modulation of the kinetic energy is sinusoidal: $E_{\text{kin}}(t) = E_{\text{kin},0} + \delta E_{\text{kin}} \sin(\omega_0 t)$.

We wrote a numerical algorithm using Python that generates a set of electron positions representing the beam. For an electron moving at $\vec{r}_\perp = (x, y)$ parallel to the z -axis and arriving at $z = 0$ at time t_j , the only non-vanishing component of the magnetic field strength at the origin becomes (take equation 11.152 from [21] and shift and rotate)

$$\vec{B}_j(0, t) = \frac{\mu_0 e \gamma v}{4\pi} \begin{bmatrix} y \\ -x \\ 0 \end{bmatrix} \frac{1}{(r_\perp^2 + \gamma^2 v^2 (t - t_j)^2)^{3/2}}. \quad (75)$$

where $\gamma = (1 - v^2/c^2)^{-1/2}$ is the Lorentz factor and $r_\perp = |\vec{r}_\perp|$. These contributions to the total magnetic field strength are summed for all electron positions. We simulated the beam over a length of $L \sim 100d$ centered at $z = 0$ to limit the numerical effort. This approximation is well justified as electrons in the beam affect the quantum system significantly only in an interaction region on the length scale of several d/γ centered at $z = 0$. For larger z , the effect

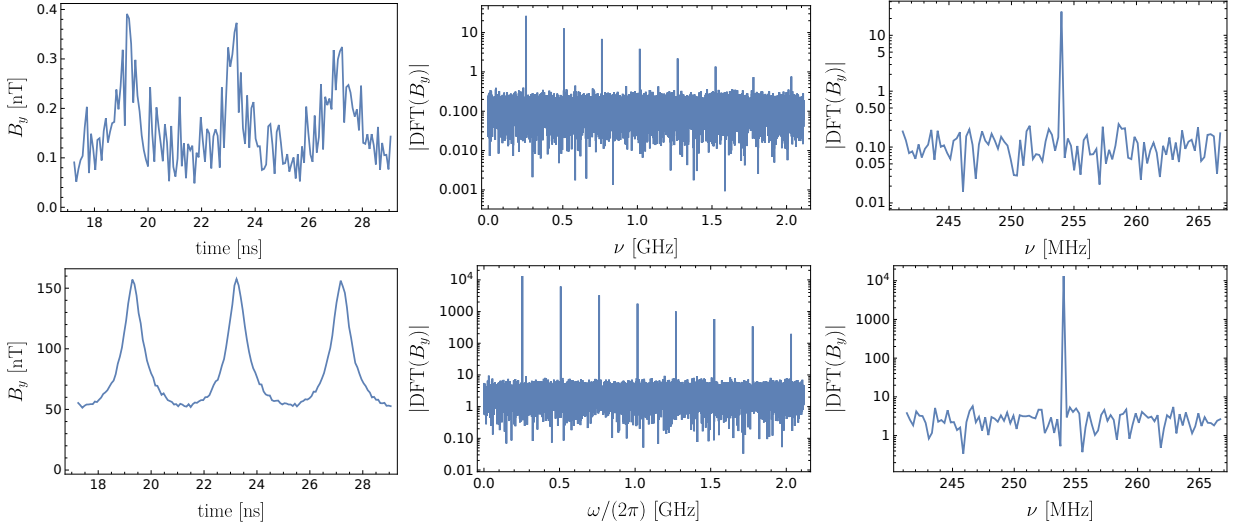


FIG. 6. Numerical simulation of the magnetic field strength B^y due to an electron beam at a distance $d = 5w = 250 \mu\text{m}$ to its center, where $w = 50 \mu\text{m}$ is the beam waist radius (left plots), and the corresponding DFT (middle and right plots) for a beam with 200 nA (upper plots) and 100 μA (lower plots). The beam current is modulated with a base frequency of $\omega = 2\pi \times 254 \text{ MHz}$ by varying the electron velocity (as e.g. in a Klystron). The higher harmonics can be seen in the middle plot. The bunching parameter r_b is approximately 0.5 ($l = 1 \text{ m}$ and $\delta E_{\text{kin}}/E_{\text{kin}} = 1/20$), which implies that the Fourier component corresponding to the modulation at base frequency has an amplitude of 50% of the average current.

on the quantum system decays as $|z|^{-3}$. The electrons have an initial kinetic energy of 18 keV. The initial transversal position of electrons is modeled as a normal distribution, where the variance $\sigma = w/2$ is given by the waist radius w of the beam. To restrict the beam to a finite radius $\Delta r_{\perp,0}$ and to avoid numerical singularities, the transversal distribution is generated from a uniform distribution by mapping values of y between 0 and 1 with the function $r_{\perp}(y) = 2^{-1/2}w\sqrt{\log((1-y)(1-\exp(-2\Delta r_{\perp,0}^2/w^2))^{-1})}$ to a radius and generating the azimuthal distribution with another uniform distribution.

Furthermore, we note that the magnetic field of each electron effectively acts on a length scale $|v(t-t_j)| \sim r_{\perp}/\gamma$ as can be seen from equation (75). Therefore, the beam divergence, specified by the divergence angle θ , can be neglected if the change of beam width is on the length scale of the interaction region $\theta r_{\perp}/\gamma \ll w$. Later, we will consider $d = 5w$, and the above condition is fulfilled for almost all electrons in the beam if $\theta \ll \gamma/5$. For a strongly focused Gaussian electron beam, θ is given by the wave properties of electrons as $\theta = \lambda_{\text{dB}}/(\pi w)$, where the de Broglie wavelength is $\lambda_{\text{dB}} = 2\pi\hbar/(\gamma m_e v)$. We obtain a condition for the waist $w \gg 10\hbar/(m_e \gamma^2 v)$. The right hand side decreases monotonously with increasing v , and, therefore, with increasing kinetic energy. For a velocity $c/4$ (corresponding to 18 keV), the right hand side becomes approximately $40\hbar/(m_e c) \sim 10^{-11} \text{ m}$, and the condition on w will be always fulfilled in the context of our proposal. For a wide beam with a given transversal kinetic energy spread of about ΔE_{kin} or less, we obtain the corresponding transversal velocity spread of $\Delta v \approx \sqrt{2\Delta E_{\text{kin}}/m_e}$ and the divergence angle $\theta = \Delta v/v$. For $v = c/4$ and $\Delta E_{\text{kin}} \sim 1 \text{ eV}$, we find $\theta \sim 10^{-2} \ll 1/5$ and the above condition is fulfilled. The results are shown in Fig.6. To generate the data for the plots, the simulation was run for 10^3 periods of the modulation.

4. THE SINGLE ELECTRON FOURIER TRANSFORM AND THE MAGNETIC FIELD SPECTRUM

The Fourier transform of the magnetic field due to the electron beam can also be calculated directly from the Fourier transform of a single electron's magnetic field. The minimal distance (impact parameter) between the electrons and the origin is $r_{\perp} := (x^2 + y^2)^{1/2}$. At time t and position $\vec{r} = 0$, the magnetic field caused by an electron moving with velocity v_j and arriving at $z = 0$ at time t_j is

$$\vec{B}_j^y(\vec{r} = 0, t) = \frac{e\mu_0\gamma_j v_j}{4\pi} \frac{r_{\perp}}{(r_{\perp}^2 + \gamma_j^2 v_j^2 (t_j - t)^2)^{3/2}}. \quad (76)$$

The temporal Fourier transform of the magnetic field of a single electron is

$$\begin{aligned}\mathcal{F}_t [B_j^y(\vec{r} = 0, t)] &= \frac{e\mu_0\gamma_j v_j}{4\pi} \frac{1}{\sqrt{2\pi}} \int_{-\infty}^{\infty} dt e^{i\omega t} \frac{r_{\perp}}{(r_{\perp}^2 + \gamma_j^2 v_j^2 (t_j - t)^2)^{3/2}} \\ &= \frac{e\mu_0}{4\pi(\gamma_j v_j)^2} \frac{1}{\sqrt{2\pi}} \int_{-\infty}^{\infty} d\tilde{t} e^{i\omega(\tilde{t}+t_j)} \frac{r_{\perp}}{((r_{\perp}^2/(\gamma_j v_j)^2 + \tilde{t}^2)^{3/2}} \\ &= \frac{e\mu_0\omega}{4\pi\gamma_j v_j} \sqrt{\frac{2}{\pi}} K_1 \left(r_{\perp} \frac{\omega}{\gamma_j v_j} \right) e^{i\omega t_j}.\end{aligned}\quad (77)$$

We note that the Fourier transform of the single electron decays exponentially for $r_{\perp}\omega/(\gamma_j v_j) \gg 1$ due to the properties of the Bessel function. For angular frequencies ω such that $r_{\perp}\omega/\gamma_j v_j \ll 1$, we can approximate $K_1(x)$ as $1/x$ and find

$$\mathcal{F}_t [B_j^y(\vec{r} = 0, t)] \approx \frac{e\mu_0}{2\pi r_{\perp}} \frac{1}{\sqrt{2\pi}} e^{i\omega t_j}.\quad (78)$$

This means that the magnetic field of a single electron appears like a delta-peak when seen on time scales much larger than $r_{\perp}/(\gamma_j v_j)$. In particular, we can conclude that the magnetic field is directly proportional to the current for these time scales.

The single electron Fourier transform can be used to obtain the discrete Fourier transform of the total magnetic field directly from our numerical model above. A plot is given in Fig.7.

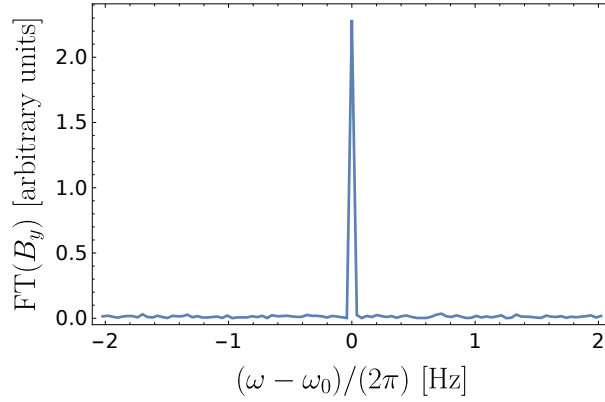


FIG. 7. Spectrum (temporal Fourier transform) of the magnetic field strength B^y due to a current modulated electron beam with 20 fA current and uniformly distributed electron positions in the longitudinal direction (z -direction) for 10^9 periods of the base frequency 254 MHz (corresponding to a total number of electrons $\sim 500\,000$). The average distance from the beamline is 5w, where $w = 1$ nm is the beam waist. The electrons have a kinetic energy of 18 keV.

To derive the expectation value of the Fourier transform of the magnetic field due to the total beam, we use the probability for an electron to pass the $z = 0$ plane at $t = t_j$, given as $\mathcal{P}(t)$. We assume that the beam has a duration T and that $\mathcal{P}(t)$ is normalized on the interval $[-T/2, T/2]$ and vanishes outside of it. Furthermore, we assume that the probability has a Fourier spectrum with distinct lines evenly spaced by ω_0 . We restrict our considerations to a one-dimensional model for the beam and set $r_{\perp} = d$. We write the Fourier decomposition as

$$\mathcal{P}(t) = \frac{1}{T} \left(a_0 + \sum_{n=-\infty}^{\infty} a_n e^{in\omega_0 t} \right) \Theta_{[-\frac{1}{2}, \frac{1}{2}]}(t),\quad (79)$$

where $\Theta_{[-\frac{1}{2}, \frac{1}{2}]}$ is the characteristic function for the interval $[-\frac{1}{2}, \frac{1}{2}]$ which takes the value one in the interval and vanishes outside of it. In particular, $\mathcal{P}(t)$ is periodic with a base frequency of ω_0 . Using the Poissonian distribution of the electron number in the interval $p_N = \bar{N}^N e^{-\bar{N}}/N!$ where $\bar{N} = E[N]$ is the expected value [70], we find

$$E[\mathcal{F}_t [B^y(\vec{r} = 0, t)]] = \frac{e\mu_0}{2\pi} \frac{1}{\sqrt{2\pi}} e^{-\bar{N}} \sum_{N=1}^{\infty} \frac{\bar{N}^N}{N!} \int \prod_{j=1}^N (dt_j \mathcal{P}(t_j)) \sum_k \frac{\omega}{\gamma_k v_k} K_1 \left(d \frac{\omega}{\gamma_k v_k} \right) e^{i\omega t_k},\quad (80)$$

where the integrals are taken over the whole sum at the end of the equation. For small bunching parameters $r_b < 1$, electrons do not overtake each other and there is a one to one correspondence of the arrival time of an electron and

its velocity, which implies $v_k = v(t_k)$ and $\gamma_k = \gamma(t_k)$. The temporally periodic modulation of the electron velocity means that $v(t_k)$ and $\gamma(t_k)$ must be periodic as well. The period is given by the base frequency ω_0 . We find

$$\begin{aligned} E[\mathcal{F}_t[B^y(\vec{r}=0, t)]] &= \frac{e\mu_0}{2\pi} \frac{1}{\sqrt{2\pi}} e^{-\bar{N}} \sum_{N=1}^{\infty} \frac{\bar{N}^N}{(N-1)!} \int_{-T/2}^{T/2} dt \mathcal{P}(t) \frac{\omega}{\gamma(t)v(t)} K_1\left(d \frac{\omega}{\gamma(t)v(t)}\right) e^{i\omega t} \\ &= \frac{e\mu_0}{2\pi} \frac{\bar{N}}{\sqrt{2\pi}} \int_{-T/2}^{T/2} dt \mathcal{P}(t) \frac{\omega}{\gamma(t)v(t)} K_1\left(d \frac{\omega}{\gamma(t)v(t)}\right) e^{i\omega t}. \end{aligned} \quad (81)$$

Due to the Bessel function K_1 decaying exponentially for arguments larger than one and $\gamma(t)$ and $v(t)$ only varying slightly in time, the spectrum of the beam will not contain frequencies much larger than $\gamma_0 v_0/d$, where v_0 and γ_0 are the average quantities. The integral in equation (81) is the Fourier transform of a $2\pi/\omega_0$ -periodic function which implies that $E[\mathcal{F}_t[B^y(\vec{r}=0, t)]]$ consists of distinct Fourier-limited spikes at multiples of ω_0 . More precisely, there exist coefficients b_n such that

$$E[\mathcal{F}_t[B^y(\vec{r}=0, t)]] = \frac{I_0\mu_0}{(2\pi)^2} \left(b_0 \frac{\sin(\omega T/2)}{\omega} + \sum_{n=-\infty}^{\infty} b_n \frac{\sin((\omega + n\omega_0)T/2)}{\omega + n\omega_0} \right), \quad (82)$$

where $I_0 = e\bar{N}/T$ is the average current. For $T \rightarrow \infty$, we have

$$E[\mathcal{F}_t[B^y(\vec{r}=0, t)]] \xrightarrow{T \rightarrow \infty} \frac{I_0\mu_0}{2\pi} \left(b_0 \delta(\omega) + \sum_{n=-\infty}^{\infty} b_n \delta(\omega + n\omega_0) \right). \quad (83)$$

The coefficients can in principle be directly calculated from equation (80). If $d\omega/(\gamma_0 v_0) \ll 1$, we can approximate the Bessel function and find

$$\begin{aligned} E[\mathcal{F}_t[B^y(\vec{r}=0, t)]] &= \frac{\mu_0}{2\pi d} \frac{\bar{N}}{\sqrt{2\pi}} \int_{-T/2}^{T/2} dt \mathcal{P}(t) e^{i\omega t} \\ &= \frac{\mu_0 I_0}{2\pi d} \frac{1}{\sqrt{2\pi}} \int_{-T/2}^{T/2} dt \left(a_0 + \sum_{n=-\infty}^{\infty} a_n e^{in\omega_0 t} \right) e^{i\omega t} \\ &= \frac{\mu_0 I_0}{2\pi d} \frac{1}{\sqrt{2\pi}} \left(a_0 \frac{\sin(\omega T/2)}{\omega} + \sum_{n=-\infty}^{\infty} a_n \frac{\sin((\omega + n\omega_0)T/2)}{\omega + n\omega_0} \right), \end{aligned} \quad (84)$$

which is proportional to the spectrum of the probability function $\mathcal{P}(t)$ that is given by the beam bunching. The average magnetic field becomes

$$\begin{aligned} E[B^y(\vec{r}=0, t)] &= \mathcal{F}_t^{-1} [E[\mathcal{F}_t[B^y(\vec{r}=0, t)]]] \\ &= \frac{\mu_0 I_0}{2\pi d} \int_{-T/2}^{T/2} dt' \left(a_0 + \sum_{n=-\infty}^{\infty} a_n e^{in\omega_0 t'} \right) \delta(t - t') \\ &= \frac{\mu_0 I_0}{2\pi d} \left(a_0 + \sum_{n=-\infty}^{\infty} a_n e^{in\omega_0 t} \right) \Theta_{[-T/2, T/2]} \\ &= \frac{\mu_0 I(t)}{2\pi d}, \end{aligned} \quad (85)$$

where $I(t) = I_0 T \mathcal{P}(t)$, which is the magnetic field of a slowly modulated one-dimensional current.

5. AUTO-COVARIANCE AND NOISE

In this section, we derive the covariance matrix of the magnetic field of a one-dimensional modulated beam

$$\begin{aligned} \text{Cov}(B_y(t), B_y(t')) &= E[B_y(t)B_y^*(t')] - E[B_y(t)]E[B_y^*(t')] \\ &= \frac{1}{2\pi} \int d\omega \int d\omega' e^{-i\omega t} e^{i\omega' t'} (E[\mathcal{F}_t[B_y](\omega)\mathcal{F}_t^*[B_y](\omega')] - E[\mathcal{F}_t[B_y](\omega)]E[\mathcal{F}_t^*[B_y](\omega')]) \\ &=: \frac{1}{2\pi} \int d\omega \int d\omega' e^{-i\omega t} e^{i\omega' t'} \text{Cov}(\mathcal{F}_t[B_y](\omega), \mathcal{F}_t[B_y](\omega')), \end{aligned} \quad (86)$$

which contains all of the information about the noise spectrum of the Gaussian random process B_y . Again, we consider a beam of N electrons with arrival times at the $z = 0$ plane that are randomly distributed over an interval T with the probability distribution $\mathcal{P}(t)$. We find

$$\begin{aligned} E[\mathcal{F}_t[B_y](\omega)\mathcal{F}^*[B_y](\omega')] &= \left(\frac{e\mu_0}{2\pi}\right)^2 e^{-\bar{N}} \left[\sum_{N=2}^{\infty} \frac{\bar{N}^N}{N!} \int \prod_{j=1}^N (dt_j \mathcal{P}(t_j)) \times \right. \\ &\times \sum_{k \neq k'} e^{i(\omega t_k - \omega' t_{k'})} \frac{\omega}{\gamma_k v_k} \frac{\omega'}{\gamma_{k'} v_{k'}} \frac{1}{2\pi} K_1\left(d \frac{\omega}{\gamma_k v_k}\right) K_1\left(d \frac{\omega'}{\gamma_{k'} v_{k'}}\right) \\ &\left. + \sum_{N=1}^{\infty} \frac{\bar{N}^N}{N!} \int \prod_{j=1}^N (dt_j \mathcal{P}(t_j)) \sum_k e^{i(\omega - \omega')t_k} \frac{\omega\omega'}{2\pi(\gamma_k v_k)^2} K_1\left(d \frac{\omega}{\gamma_k v_k}\right) K_1\left(d \frac{\omega'}{\gamma_k v_k}\right) \right]. \end{aligned} \quad (87)$$

Again for bunching parameters $r_b < 1$, we can write

$$\begin{aligned} E[\mathcal{F}_t[B_y](\omega)\mathcal{F}^*[B_y](\omega')] &= \left(\frac{e\mu_0}{2\pi}\right)^2 \left[\bar{N}^2 \int_{-T/2}^{T/2} dt \mathcal{P}(t) \int_{-T/2}^{T/2} dt' \mathcal{P}(t') \times \right. \\ &e^{i(\omega t - \omega' t')} \frac{\omega}{\gamma(t)v(t)} \frac{\omega'}{\gamma(t')v(t')} \frac{1}{2\pi} K_1\left(d \frac{\omega}{\gamma v}\right) K_1\left(d \frac{\omega'}{\gamma v'}\right) \\ &\left. + \bar{N} \int_{-T/2}^{T/2} dt \mathcal{P}(t) e^{i(\omega - \omega')t} \frac{\omega\omega'}{2\pi(\gamma(t)v(t))^2} K_1\left(d \frac{\omega}{\gamma(t)v(t)}\right) K_1\left(d \frac{\omega'}{\gamma(t)v(t)}\right) \right]. \end{aligned} \quad (88)$$

Subtracting the square of the expectation value of the spectrum, we obtain

$$\begin{aligned} \text{Cov}(\mathcal{F}_t[B_y](\omega), \mathcal{F}_t[B_y](\omega')) &= \\ &\left(\frac{e\mu_0}{2\pi}\right)^2 \bar{N} \int_{-T/2}^{T/2} dt \mathcal{P}(t) e^{i(\omega - \omega')t} \frac{\omega\omega'}{2\pi(\gamma(t)v(t))^2} K_1\left(d \frac{\omega}{\gamma(t)v(t)}\right) K_1\left(d \frac{\omega'}{\gamma(t)v(t)}\right). \end{aligned} \quad (89)$$

This implies that the variance of the spectrum (for $T \gg 1/\omega_0$) is

$$\text{Var}_{B_y}(\omega) = \text{Cov}(B_y(\omega), B_y(\omega)) = \left(\frac{e\mu_0}{2\pi}\right)^2 \bar{N} \int_{-T/2}^{T/2} dt \mathcal{P}(t) \frac{\omega^2}{2\pi(\gamma(t)v(t))^2} \left(K_1\left(d \frac{\omega}{\gamma(t)v(t)}\right)\right)^2. \quad (90)$$

In particular,

$$S_{B_y B_y}(\omega) = \frac{1}{T} \left(E[\mathcal{F}_t[B_y](\omega)]^2 + \text{Var}_{B_y}(\omega) \right) \quad (91)$$

is the power spectral density. Our result shows that the average spectrum is not changed by the fluctuation, but that there is just a noise floor that is homogeneous for frequencies $\omega \ll \gamma v/d$ and falls off quickly for $\omega \gg \gamma v/d$. For $\omega \ll \gamma v/d$, we find

$$\text{Var}_{B_y}(\omega) = \left(\frac{e\mu_0}{2\pi d}\right)^2 \frac{\bar{N}}{2\pi}. \quad (92)$$

Furthermore, from equation (89) we obtain

$$\text{Cov}(\mathcal{F}_t[B_y](\omega), \mathcal{F}_t[B_y](\omega')) = \left(\frac{e\mu_0}{2\pi d}\right)^2 \frac{\bar{N}}{2\pi} \int_{-T/2}^{T/2} dt \mathcal{P}(t) e^{i(\omega - \omega')t}. \quad (93)$$

We can calculate the temporal auto covariance with the two point Fourier transform of (89), with which we find

$$\text{Cov}(B_y(t), B_y(t')) = \left(\frac{e\mu_0}{2\pi d}\right)^2 \frac{I(t)}{e} \delta(t - t') \Theta_{[-\frac{1}{2}, \frac{1}{2}]} \left(\frac{t}{T}\right). \quad (94)$$

We find that we are dealing with delta correlated noise. Introducing a frequency cut-off such that $\delta(t - t') \rightarrow \Delta f$, we find

$$\text{Var}(B_y(t)) = \left(\frac{\mu_0}{2\pi d}\right)^2 e I(t) \Delta f. \quad (95)$$

This implies $\text{Var}(B_y(t))/E[B_y(t)]^2 = e\Delta f/I(t)$ which is the signature of shot-noise. Equating $1/\Delta f$ with the time scale of the interaction of electron and quantum system $d/\gamma v$, we find that the signal to noise ratio $\text{Var}_{B_y}(t)/E[B_y(t)]^2$ is small if

$$\frac{\gamma v e}{I(t)d} \ll 1. \quad (96)$$

The condition in equation (96) must be fulfilled to obtain a continuous driving signal with small noise. The factor $d/\gamma v$ can be identified as the inverse auto-correlation time τ_c as it is the inverse of the frequency scale on which the auto-covariance in equation (89) decays. Thus, the condition in equation (96) simplifies to $I_{\min}\tau_c/e \gg 1$, where I_{\min} is the minimal value of the modulated current. This implies that a continuous signal with small noise is ensured if there are many electrons passing the quantum system per auto-correlation time. Assuming a kinetic energy of 18 keV and a minimal current of $I_{\min} = 20 \mu\text{A}$, we obtain a required distance of the quantum system to the center of the beamline of $d \gg 600 \text{ nm}$. Note that this condition is not a general limit of the mechanism we propose but only of the applicability of the approximation of a continuous driving signal with small noise. If the condition is not fulfilled, then a different model must be chosen. In the case of quantum systems being driven by the magnetic field of single well separated electrons, we simulate the time evolution of the state of the quantum system for each electron separately; details can be found below in Sec.12.

6. THE AVERAGED MAGNETIC FIELD SEEN BY THE QUANTUM SYSTEM

In the following section, we assume that the distance of the quantum system to the center of the beam d is much smaller than the wavelength of the beam modulation $\lambda_0 = 2\pi v/\omega_0$ and that the waist w of the beam is much smaller than d . Based on the magnetic field due to a single electron in equation (75), the magnetic field induced by an infinitesimal segment of a one-dimensional beam can be written as

$$d\vec{B}_j(0, t) = \frac{\mu_0 \gamma I(z, t) dz'}{4\pi} \begin{bmatrix} y \\ -x \\ 0 \end{bmatrix} \frac{1}{(r_{\perp}^2 + \gamma^2 z^2)^{3/2}}. \quad (97)$$

Then, for the whole beam, we write

$$\vec{B}_j(0, t) = \int d\vec{B}_j(0, t) = \int_{-\infty}^{\infty} dz \frac{\mu_0 I(z, t)}{4\pi\gamma^2} \begin{bmatrix} y \\ -x \\ 0 \end{bmatrix} \frac{1}{(r_{\perp}^2/\gamma^2 + z^2)^{3/2}}. \quad (98)$$

The integrand is localized to a region of length r_{\perp}/γ . If $I(z, t)$ does not change significantly on this length scale, we can approximate

$$\vec{B}_j(0, t) \rightarrow \int_{-\infty}^{\infty} dz \frac{\mu_0 I(z, t)}{4\pi\gamma^2} \begin{bmatrix} y \\ -x \\ 0 \end{bmatrix} \frac{2\gamma^2}{r_{\perp}^2} \delta(z) = \frac{\mu_0 I(0, t)}{2\pi r_{\perp}^2} \begin{bmatrix} y \\ -x \\ 0 \end{bmatrix}. \quad (99)$$

For the current of the specific case of the Klystron beam, we have the Fourier decomposition

$$I(z, t) = I_0 \left[1 + \sum_{n=1}^{\infty} 2J_n(n r_b(z)) \cos \left(n\omega_0 \left(t - \frac{(z - z_0)}{v_0} \right) \right) \right], \quad (100)$$

Restricting our considerations to the Fourier component at the base frequency ω_0 , from the condition that $I(z, t)$ does not change significantly on the length scale r_{\perp}/γ , we obtain the conditions $r_{\perp} \ll \gamma\lambda_0 = 2\pi\gamma v_0/\omega_0$ and

$$r_{\perp}/\gamma \ll \frac{J_1(r_b(z))}{dJ_1(r_b(z))/dz} = \frac{J_1(r_b(z))}{J_1'(r_b(z)) dr_b(z)/dz}. \quad (101)$$

For the bunching parameter $r_b(z) \leq 1$, we have $J_1(r_b)/J_1'(r_b) \sim r_b$ and the second condition becomes $r_{\perp} \ll \gamma l$. Therefore, we consider a non-divergent beam with a Gaussian profile $j_e(\vec{r}, t) = \hat{z} 2I(t) \exp(-2|\vec{r}_{\perp} - \vec{r}_{\perp,0}|^2/w^2)/(\pi w^2)$. $j_e(\vec{r})$ is normalized such that $I(t)$ is the average current obtained by integrating the charge density over the x - y plane,

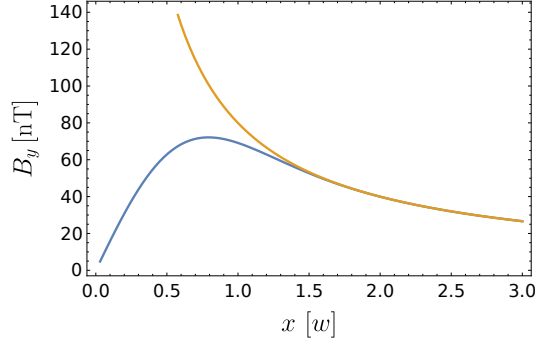


FIG. 8. The time-averaged magnetic field strength due to an electron beam with an averaged current of $20 \mu\text{A}$ as a function of the distance x in units of the waist w from the beam's center ($y = 0$) for a Gaussian (blue) and an infinitely thin (orange) electron beam.

and $\vec{r}_{\perp,0}$ is the position of the beam's center, i.e. $|\vec{r}_{\perp,0}| = d$. The parameter w is the waist radius of the beam such that the beam has a $1/e^2$ -diameter of $2w$. Under the conditions above, we obtain

$$E[\vec{B}(t)] = \frac{\mu_0 I(t)}{\pi^2 w^2} \int d^2 r_{\perp} \begin{bmatrix} y \\ -x \\ 0 \end{bmatrix} \frac{e^{-\frac{2|\vec{r}_{\perp} - \vec{r}_{\perp,0}|^2}{w^2}}}{r_{\perp}^2}. \quad (102)$$

Equation (102) gives the general result for distances to the beam $d \ll \lambda$. If additionally $d > 2w$ holds, one can easily verify that the magnetic field strength of a Gaussian beam can be well approximated by that of an infinitely thin beam. A plot demonstrating this is shown in Fig.8.

7. THE OPTICAL BLOCH EQUATIONS

To derive the description of the quantum system, we start from the interaction Hamiltonian in the Coulomb gauge

$$\hat{H}_{\text{int}} = -\vec{\mu} \cdot \vec{B}, \quad (103)$$

where $\vec{B}(t) = (B_x(t), B_y(t), B_z(t))$ and $\vec{\mu} = \vec{\mu}_L + \vec{\mu}_S + \vec{\mu}_I$, where $\vec{\mu}_L = -\mu_B g_L \vec{L}/\hbar$, $\vec{\mu}_S = -\mu_B g_S \vec{S}/\hbar$ and $\vec{\mu}_I = \mu_N g_I \vec{I}/\hbar$. $\mu_B = e\hbar/(2m_e)$ is the Bohr magneton, $g_L = 1 - m_e/m_n \approx 1$ is the orbital gyromagnetic ratio, $g_S \approx 2$ is the spin gyromagnetic ratio, $\mu_N = e\hbar/(2m_p)$ is the nuclear magneton and g_I is the total nuclear gyromagnetic ratio. The quantum system is considered as a two level system with the free Hamiltonian $H_0 = \hbar\omega_0\sigma_z/2$. For the time evolution of the density matrix ρ , we consider the Lindblad equation

$$\partial_t \rho = \frac{1}{i\hbar} [\hat{H}_0 + \hat{H}_{\text{int}}, \rho] + \Gamma \left(\hat{L} \rho \hat{L}^\dagger - \frac{1}{2} \hat{L}^\dagger \hat{L} \rho - \frac{1}{2} \rho \hat{L}^\dagger \hat{L} \right), \quad (104)$$

with the Lindblad operator $\hat{L} = |g\rangle\langle e|$ representing the spontaneous emission into the radiation field corresponding to the natural linewidth of the transition. We obtain

$$\left(i\hbar \frac{d}{dt} - \begin{bmatrix} \hbar\omega_0 - i\hbar\frac{\Gamma}{2} & 0 & -T_{ge}^* & T_{ge}^* \\ 0 & -\hbar\omega_0 - i\hbar\frac{\Gamma}{2} & T_{ge} & -T_{ge} \\ -T_{ge} & T_{ge}^* & -i\hbar\Gamma & 0 \\ T_{ge} & -T_{ge}^* & i\hbar\Gamma & 0 \end{bmatrix} \right) \begin{bmatrix} \rho_{eg}(t) \\ \rho_{ge}(t) \\ \rho_{ee}(t) \\ \rho_{gg}(t) \end{bmatrix} = 0, \quad (105)$$

where $T_{ge} = \langle g|H_{\text{int}}|e\rangle$ is the time dependent transition moment from the excited to the ground state. With the transformation $\tilde{\rho}_{eg}(t) = \rho_{eg}(t)e^{i\omega_0 t}$, $\tilde{\rho}_{ge}(t) = \rho_{ge}(t)e^{-i\omega_0 t}$, $\tilde{\rho}_{ee}(t) = \rho_{ee}(t)$ and $\tilde{\rho}_{gg}(t) = \rho_{gg}(t)$, we find

$$\left(i\hbar \frac{d}{dt} - \begin{bmatrix} -i\hbar\frac{\Gamma}{2} & 0 & -T_{ge}^* e^{i\omega_0 t} & T_{ge}^* e^{i\omega_0 t} \\ 0 & -i\hbar\frac{\Gamma}{2} & T_{ge} e^{-i\omega_0 t} & -T_{ge} e^{-i\omega_0 t} \\ -T_{ge} e^{-i\omega_0 t} & T_{ge}^* e^{i\omega_0 t} & -i\hbar\Gamma & 0 \\ T_{ge} e^{-i\omega_0 t} & -T_{ge}^* e^{i\omega_0 t} & i\hbar\Gamma & 0 \end{bmatrix} \right) \begin{bmatrix} \tilde{\rho}_{eg}(t) \\ \tilde{\rho}_{ge}(t) \\ \tilde{\rho}_{ee}(t) \\ \tilde{\rho}_{gg}(t) \end{bmatrix} = 0. \quad (106)$$

This equation corresponds to the case that the coherence time is given as $T_2 = 2T_1 = 2/\Gamma$ which can be seen by the term $\Gamma/2$ appearing in the components of the matrix operator governing the decay of the off-diagonal elements of the density matrix. The generalization to general T_2 becomes (see Sec.4 of [23] and set $\gamma_a = \Gamma_1$, $\gamma_b = 0$ and $\gamma_{\text{ph}} = \Gamma_2 - \Gamma_1/2$ and taking into account that the upper level decays into the lower level leading to equation (4.31))

$$\left(i\hbar \frac{d}{dt} - \begin{bmatrix} -i\hbar\Gamma_2 & 0 & -T_{ge}^* e^{i\omega_0 t} & T_{ge}^* e^{i\omega_0 t} \\ 0 & -i\hbar\Gamma_2 & T_{ge} e^{-i\omega_0 t} & -T_{ge} e^{-i\omega_0 t} \\ -T_{ge} e^{-i\omega_0 t} & T_{ge}^* e^{i\omega_0 t} & -i\hbar\Gamma_1 & 0 \\ T_{ge} e^{-i\omega_0 t} & -T_{ge}^* e^{i\omega_0 t} & i\hbar\Gamma_1 & 0 \end{bmatrix} \right) \begin{bmatrix} \tilde{\rho}_{eg}(t) \\ \tilde{\rho}_{ge}(t) \\ \tilde{\rho}_{ee}(t) \\ \tilde{\rho}_{gg}(t) \end{bmatrix} = 0, \quad (107)$$

where $\Gamma_j = 1/T_j$ and $j \in \{1, 2\}$. With $B_i(t) = (\mathcal{B}_i e^{-i\omega_M t} + c.c.)/2$, we can consider on-resonance driving such that $\omega_M = \omega_0$, and use the rotating wave approximation to find

$$\left(\frac{d}{dt} - \begin{bmatrix} -\Gamma_2 & 0 & -i\Omega/2 & i\Omega/2 \\ 0 & -\Gamma_2 & i\Omega^*/2 & -i\Omega^*/2 \\ -i\Omega^*/2 & i\Omega/2 & -\Gamma_1 & 0 \\ i\Omega^*/2 & -i\Omega/2 & \Gamma_1 & 0 \end{bmatrix} \right) \begin{bmatrix} \tilde{\rho}_{eg}(t) \\ \tilde{\rho}_{ge}(t) \\ \tilde{\rho}_{ee}(t) \\ \tilde{\rho}_{gg}(t) \end{bmatrix} = 0, \quad (108)$$

where we define the complex Rabi frequency as

$$\Omega = -\langle e | \vec{\mu} | g \rangle \cdot \vec{\mathcal{B}} / \hbar, \quad (109)$$

where $\vec{\mathcal{B}} = (\mathcal{B}_x, \mathcal{B}_y, \mathcal{B}_z)$.

The finite spectral linewidth of the electromagnetic near-field created by the electron beam will influence the evolution of the quantum system. For the interaction of atoms with laser light, this has been investigated in [24–28]. For the case of a modulated current with small fluctuations relative to the mean (e.g. shot noise, modulation phase noise), the result can be applied immediately due to the equivalence of the interaction Hamiltonian. With the resonance condition, the rotating wave approximation leads to the modified optical Bloch equations

$$0 = \left(\frac{d}{dt} - \begin{bmatrix} -\Gamma_2 - b & 0 & -i\Omega/2 & i\Omega/2 \\ 0 & -\Gamma_2 - b & i\Omega/2 & -i\Omega/2 \\ -i\Omega/2 & i\Omega/2 & -\Gamma_1 & 0 \\ i\Omega/2 & -i\Omega/2 & \Gamma_1 & 0 \end{bmatrix} \right) \begin{bmatrix} \tilde{\rho}_{eg}^1 \\ \tilde{\rho}_{ge}^{-1} \\ \tilde{\rho}_{ee}^0 \\ \tilde{\rho}_{gg}^0 \end{bmatrix} \quad (110)$$

for $\tilde{\rho}_{ij}^k(t) := \langle \tilde{\rho}_{ij}(t) \exp(ik\phi(t)) \rangle_{\text{ph}}$, which are the components of the quantum system's density matrix averaged over the phase noise $\phi(t)$, representing the finite spectral linewidth. The damping rate b in equation (110) is related to the Full Width at Half Maximum (FWHM) linewidth $\delta\omega$ of the modulation as $b = \delta\omega/2$ as we will show in the following.

FWHM linewidth and coherence length

In [24], the inverse coherence length b is defined via $\langle \exp(i\phi(t)) \exp(-i\phi(t')) \rangle = \exp(-b|t - t'|)$. The magnetic field is given by its Fourier transform as

$$B(t) = \int \frac{d\omega}{2\pi} e^{i\omega t} \hat{B}(\omega). \quad (111)$$

Therefore, the cross correlation becomes ($E[\dots]$ denoting the expected value)

$$E[B^*(t)B(t + \tau)] = \int_{-\infty}^{\infty} dt B^*(t)B(t + \tau) \quad (112)$$

$$= \int_{-\infty}^{\infty} dt \int \frac{d\omega}{2\pi} e^{-i\omega t} \hat{B}(\omega)^* \int \frac{d\omega'}{2\pi} e^{i\omega'(t+\tau)} \hat{B}(\omega') \quad (113)$$

$$= \int \frac{d\omega}{2\pi} e^{i\omega\tau} |\hat{B}(\omega)|^2. \quad (114)$$

If a Lorentzian line shape is given, and

$$|\hat{B}(\omega)|^2 \propto \frac{(\delta\omega/2)^2}{(\omega_0 - \omega)^2 + (\delta\omega/2)^2}, \quad (115)$$

where $\delta\omega$ is the FWHM linewidth in rad/s, we find

$$E[B^*(t)B(t+\tau)] \propto e^{-\frac{\delta\omega}{2}\tau} e^{i\omega_0\tau}. \quad (116)$$

This implies that the inverse coherence length is $b = \delta\omega/2$.

8. TRANSITION MATRIX ELEMENTS FOR ^{41}K

For Potassium-41, we have $g_S \approx 2$ and $g_I \approx -0.000078$. Therefore, we will only consider the coupling of the external magnetic field to the electron spin in the following section. For a hyperfine transition, we can simplify T_{ge} as

$$T_{ge} = \mu_B g_S \langle e | \vec{S} | g \rangle \cdot \vec{B} / \hbar. \quad (117)$$

For the case that the magnetic field has only one non-zero component, e.g. the B_y -component, we can write

$$T_{ge} = \mu_B g_S \langle e | S_y | g \rangle B_y / \hbar. \quad (118)$$

Using the y -direction as the quantization direction and taking into account that, for the $F = 2$ hyperfine state and $m_F = 0$ Zeeman sub-level,

$$|F = 2, m_F = 0\rangle = \sqrt{\frac{1}{2}} \left| \frac{3}{2}, \frac{1}{2} \right\rangle \left| \frac{1}{2}, -\frac{1}{2} \right\rangle + \sqrt{\frac{1}{2}} \left| \frac{3}{2}, -\frac{1}{2} \right\rangle \left| \frac{1}{2}, \frac{1}{2} \right\rangle \quad (119)$$

and for the $F = 1$ and $m_F = 0$,

$$|F = 1, m_F = 0\rangle = \sqrt{\frac{1}{2}} \left| \frac{3}{2}, \frac{1}{2} \right\rangle \left| \frac{1}{2}, -\frac{1}{2} \right\rangle - \sqrt{\frac{1}{2}} \left| \frac{3}{2}, -\frac{1}{2} \right\rangle \left| \frac{1}{2}, \frac{1}{2} \right\rangle, \quad (120)$$

we obtain

$$\begin{aligned} T_{ge} &= \frac{\mu_B B_y}{\hbar} \langle F = 2, m_F = 0 | g_L L_y + g_S S_y | F = 1, m_F = 0 \rangle \\ &= \frac{\mu_B g_S B_y}{\hbar} \langle F = 2, m_F = 0 | S_y \left(\sqrt{\frac{1}{2}} \left| \frac{3}{2}, \frac{1}{2} \right\rangle \left| \frac{1}{2}, -\frac{1}{2} \right\rangle - \sqrt{\frac{1}{2}} \left| \frac{3}{2}, -\frac{1}{2} \right\rangle \left| \frac{1}{2}, \frac{1}{2} \right\rangle \right) \rangle = -\frac{\mu_B g_S B_y}{2}. \end{aligned} \quad (121)$$

and $\tilde{T}_{ge}/\hbar = -e^{-i\omega_0 t} g_S \mu_B B_y / (2\hbar) \approx -e^{-i\omega_0 t} e B_y / (2m_e)$, where e is the unit charge and m_e is the electron mass. For the Rabi frequency, we thus find

$$\Omega \approx \frac{g_S \mu_B B_y}{2\hbar} \approx \frac{e B_y}{2m_e}. \quad (122)$$

9. TRANSITION MATRIX ELEMENTS FOR NV CENTERS

The transition between the 3A_2 ground state magnetic sublevels $m_s = 0$ and $m_s = \pm 1$ is a mutual polarization of two half-filled molecular orbitals. However, the spin triplet $m_s = 0$ and $m_s = \pm 1$ can be described as an effective single spin 1 system with the coupling to an external magnetic field [38, 71]

$$H_{\text{int}} = g_S \mu_B \vec{S} \cdot \vec{B} / \hbar. \quad (123)$$

We consider the x -direction as the quantization direction. The spin operator $\vec{S} = (S_x, S_y, S_z)$ acts on the fine-structure sub-levels such that $S_x |m_s\rangle = \hbar m_s |m_s\rangle$ and for $S_{\pm} = S_y \pm iS_z$, we have

$$S_{\pm} |m_s\rangle = \hbar \sqrt{2 - m_s(m_s \pm 1)} |m_s \pm 1\rangle. \quad (124)$$

We consider the magnetic field oriented in the y -direction. Then,

$$T_{ge} = \frac{g_S \mu_B B_y}{2\hbar} \langle \pm 1 | (S_+ + S_-) | 0 \rangle = \frac{g_S \mu_B B_y}{\sqrt{2}}. \quad (125)$$

and $\tilde{T}_{ge} = e^{-i\omega_0 t} g_S \mu_B B_y / \sqrt{2}$.

10. THE OPTICAL BLOCH EQUATIONS WITH SHOT NOISE

We start with the optical Bloch equations before the rotating frame transformation and neglecting damping:

$$\frac{d}{dt} \begin{bmatrix} \rho_{eg}(t) \\ \rho_{ge}(t) \\ \rho_{ee}(t) \\ \rho_{gg}(t) \end{bmatrix} = -i \begin{bmatrix} \omega_0 & 0 & -T_{ge}/\hbar & T_{ge}/\hbar \\ 0 & -\omega_0 & T_{ge}/\hbar & -T_{ge}/\hbar \\ -T_{ge}/\hbar & T_{ge}/\hbar & 0 & 0 \\ T_{ge}/\hbar & -T_{ge}/\hbar & 0 & 0 \end{bmatrix} \begin{bmatrix} \rho_{eg}(t) \\ \rho_{ge}(t) \\ \rho_{ee}(t) \\ \rho_{gg}(t) \end{bmatrix}. \quad (126)$$

For the sake of simplicity, we assume real transition matrix elements, that is $T_{ge}/\hbar = T_{ge}^*/\hbar$. From equation (121), we have $T_{ge}/\hbar = -eB_y/(2m_e)$ for the transition we consider. Furthermore, we consider the situation where $d/\gamma v$ is much smaller than all time scales under consideration, such that we can approximate the average field as equation (85) and its covariance as equation (95). We can write equation (126) as

$$\dot{u} = (\mathbf{B}_0 + \alpha \mathbf{B}_1(t, \xi))u, \quad (127)$$

where $u = (\rho_{eg}(t), \rho_{ge}(t), \rho_{ee}(t), \rho_{gg}(t))$ and

$$\mathbf{B}_0 = i\omega_0 \begin{bmatrix} -1 & 0 & 0 & 0 \\ 0 & 1 & 0 & 0 \\ 0 & 0 & 0 & 0 \\ 0 & 0 & 0 & 0 \end{bmatrix}, \quad \mathbf{B}_1 = i \frac{T_{ge}}{\hbar \alpha} \mathbf{M} \quad \text{and} \quad \mathbf{M} = \begin{bmatrix} 0 & 0 & 1 & -1 \\ 0 & 0 & -1 & 1 \\ 1 & -1 & 0 & 0 \\ -1 & 1 & 0 & 0 \end{bmatrix}. \quad (128)$$

α is a parameter estimating the magnitude of fluctuations, which in our case implies

$$\alpha \sim T_{ge}(t, \xi)/\hbar - E[T_{ge}(t, \xi)]/\hbar. \quad (129)$$

With equation (95) and the frequency scale $\Delta f \sim \gamma v/d$, this equation implies

$$\alpha \sim \frac{e}{2m_e} \sqrt{\max_t (\text{Var}(B_y(t, \xi)))} \sim \frac{e^2 \mu_0}{4\pi m_e d} \sqrt{\frac{I_{\max} \gamma v}{e}}. \quad (130)$$

In the following, we will derive an ordinary linear differential equation for the expectation value of the vector of components of the density matrix u given in [30]. To this end, we must assume that $\alpha \tau_c \ll 1$, where τ_c is the auto-correlation time of the magnetic field. If this condition is fulfilled, then the ensemble average of u fulfills the integro-differential equation (see [30])

$$\frac{d}{dt} E[u(t)] = (\mathbf{K}_0 + \alpha \mathbf{K}_1(t) + \alpha^2 \mathbf{K}_2(t)) E[u(t)] \quad (131)$$

where $\mathbf{K}_0 = \mathbf{B}_0$,

$$\mathbf{K}_1(t) = E[\mathbf{B}_1(t, \xi)] = i \frac{E[T_{ge}]}{\hbar \alpha} \mathbf{M}, \quad (132)$$

$$\mathbf{K}_2(t) = \int_0^\infty dt' \langle\langle \mathbf{K}_1(t) \mathbf{Y}(t|t') \mathbf{K}_1(t') \rangle\rangle \mathbf{Y}(t'|t) \quad (133)$$

where we consider times much larger than the correlation time τ_c , and the matrix $\mathbf{Y}(t, t')$ is the time-evolution operator for the differential equation

$$\begin{aligned} \frac{d}{dt} E[u(t)] &= (\mathbf{K}_0 + \alpha \mathbf{K}_1(t)) E[u(t)] \\ &= (\mathbf{B}_0 + \alpha E[\mathbf{B}_1(t, \xi)]) E[u(t)]. \end{aligned} \quad (134)$$

$\langle\langle \dots \rangle\rangle$ denotes the cumulant, and therefore

$$\begin{aligned} \langle\langle \mathbf{K}_1(t) \mathbf{Y}(t|t') \mathbf{K}_1(t') \rangle\rangle &= E[\mathbf{K}_1(t) \mathbf{Y}(t|t') \mathbf{K}_1(t')] - E[\mathbf{K}_1(t)] \mathbf{Y}(t|t') E[\mathbf{K}_1(t')] \\ &= -\frac{1}{(\hbar \alpha)^2} (E[T_{ge}(t) T_{ge}(t')] - E[T_{ge}(t)] E[T_{ge}(t')]) \mathbf{M} \cdot \mathbf{Y}(t|t') \cdot \mathbf{M} \\ &= -\frac{1}{(\hbar \alpha)^2} \text{Cov}(T_{ge}(t), T_{ge}(t')) \mathbf{M} \cdot \mathbf{Y}(t|t') \cdot \mathbf{M}. \end{aligned} \quad (135)$$

On the time scale of ω_0 , the driving T_{ge} can be assumed to be delta-correlated. In particular, for $1/\omega_0 \gg \tau_c$, we can set $\text{Cov}(T_{ge}(t), T_{ge}(t')) = \hbar^2 a I(t) I_0^{-1} \delta(t - t')$ based on equation (94), where $a = (e^2 \mu_0)^2 I_0 / ((4\pi m_e d)^2 e)$. As $\mathbf{Y}(t|t') = \mathbb{I}$, we obtain

$$\langle\langle \mathbf{K}_1(t) \mathbf{Y}(t|t') \mathbf{K}_1(t') \rangle\rangle = -\frac{aI(t)}{\alpha^2 I_0} \delta(t - t') \mathbf{M} \cdot \mathbf{M}, \quad (136)$$

and

$$\alpha^2 \mathbf{K}_2(t) = -\frac{2aI(t)}{I_0} \begin{bmatrix} 1 & -1 & 0 & 0 \\ -1 & 1 & 0 & 0 \\ 0 & 0 & 1 & -1 \\ 0 & 0 & -1 & 1 \end{bmatrix}. \quad (137)$$

Finally,

$$\frac{d}{dt} \begin{bmatrix} \rho_{eg}(t) \\ \rho_{ge}(t) \\ \rho_{ee}(t) \\ \rho_{gg}(t) \end{bmatrix} = \begin{bmatrix} -i\omega_0 - \frac{2aI(t)}{I_0} & \frac{2aI(t)}{I_0} & iE[T_{ge}]/\hbar & -iE[T_{ge}]/\hbar \\ \frac{2aI(t)}{I_0} & i\omega_0 - \frac{2aI(t)}{I_0} & -iE[T_{ge}]/\hbar & iE[T_{ge}]/\hbar \\ iE[T_{ge}]/\hbar & -iE[T_{ge}]/\hbar & -\frac{2aI(t)}{I_0} & \frac{2aI(t)}{I_0} \\ -iE[T_{ge}]/\hbar & iE[T_{ge}]/\hbar & \frac{2aI(t)}{I_0} & -\frac{2aI(t)}{I_0} \end{bmatrix} \begin{bmatrix} \rho_{eg}(t) \\ \rho_{ge}(t) \\ \rho_{ee}(t) \\ \rho_{gg}(t) \end{bmatrix}. \quad (138)$$

Taking into account that $I(t)$ has a spectrum with distinct lines and a large spacing between spectral lines ω_0 , the transformation to the rotating frame, the RWA and averaging the damping lead to

$$\frac{d}{dt} \begin{bmatrix} \tilde{\rho}_{eg}(t) \\ \tilde{\rho}_{ge}(t) \\ \tilde{\rho}_{ee}(t) \\ \tilde{\rho}_{gg}(t) \end{bmatrix} = \begin{bmatrix} -2a & 0 & -i\Omega_0/2 & i\Omega_0/2 \\ 0 & -2a & i\Omega_0/2 & -i\Omega_0/2 \\ -i\Omega_0/2 & i\Omega_0/2 & -2a & 2a \\ i\Omega_0/2 & -i\Omega_0/2 & 2a & -2a \end{bmatrix} \begin{bmatrix} \tilde{\rho}_{eg}(t) \\ \tilde{\rho}_{ge}(t) \\ \tilde{\rho}_{ee}(t) \\ \tilde{\rho}_{gg}(t) \end{bmatrix}. \quad (139)$$

where $\Omega_0 = -e\mu_0 I_{\omega_0} / (4\pi m_e d)$, where $I_{\omega_0} = 2I_0 J_1(r_b(z))$ is the Fourier coefficient of the modulation at the base frequency (see equation 74). This can be reformulated as

$$\frac{d}{dt} \begin{bmatrix} \tilde{\rho}_{eg}(t) - \tilde{\rho}_{ge}(t) \\ \tilde{\rho}_{eg}(t) + \tilde{\rho}_{ge}(t) \\ \tilde{\rho}_{ee}(t) - \tilde{\rho}_{gg}(t) \\ \tilde{\rho}_{ee}(t) + \tilde{\rho}_{gg}(t) \end{bmatrix} = \begin{bmatrix} -2a & 0 & -i\Omega_0 & 0 \\ 0 & -2a & 0 & 0 \\ -i\Omega_0 & 0 & -4a & 0 \\ 0 & 0 & 0 & 0 \end{bmatrix} \begin{bmatrix} \tilde{\rho}_{eg}(t) - \tilde{\rho}_{ge}(t) \\ \tilde{\rho}_{eg}(t) + \tilde{\rho}_{ge}(t) \\ \tilde{\rho}_{ee}(t) - \tilde{\rho}_{gg}(t) \\ \tilde{\rho}_{ee}(t) + \tilde{\rho}_{gg}(t) \end{bmatrix}. \quad (140)$$

We find that shot noise leads to additional decoherence terms and an additional damping term proportional to a in the optical Bloch equations. If we want to ignore this damping, then we have to fulfill the condition

$$4a = \left(\frac{e^2 \mu_0}{4\pi m_e d} \right)^2 \frac{4I_0}{e} \ll \Omega_0 = \frac{e\mu_0 I_{\omega_0}}{4\pi m_e d}, \quad (141)$$

which leads to the general condition

$$d \gg \frac{e^2 \mu_0 I_0}{\pi m_e I_{\omega_0}} = \frac{2\lambda_e \alpha_{\text{FS}} I_0}{\pi I_{\omega_0}} \quad (142)$$

where λ_e is the electron's Compton wave length and α_{FS} is the fine structure constant. Since $\lambda_e \alpha_{\text{FS}} \sim 10^{-14}$ m, the above condition can always be fulfilled in the context of this article.

For the method we used above to be applicable, we had to assume that $\alpha\tau_c \ll 1$, where we identified $\tau_c \sim d/(\gamma v)$. We obtain

$$\alpha_c \tau_c \sim \frac{\lambda_e \alpha_{\text{FS}}}{2\pi} \sqrt{\frac{I_{\text{max}}}{e d \gamma v}}, \quad (143)$$

from which we find the condition for the distance

$$d \gg \left(\frac{\lambda_e \alpha_{\text{FS}}}{2\pi} \right)^2 \frac{I_{\text{max}}}{e \gamma v}. \quad (144)$$

For a kinetic energy of 18 keV and an average current of $I_0 = 50 \mu\text{A}$, we find the right hand side of this condition to be on the order of 10^{-21} m. Therefore, this condition can be fulfilled for the situation that we consider. Since a larger current leads to a reduced noise to signal ratio of the magnetic field, it seems counter-intuitive that the minimal distance between beam line and quantum system grows with the current. However, the above condition only applies to the method presented in [30].

11. EXAMPLE 1: DRIVING GROUND STATE HYPERFINE TRANSITIONS IN ALKALI ATOMS

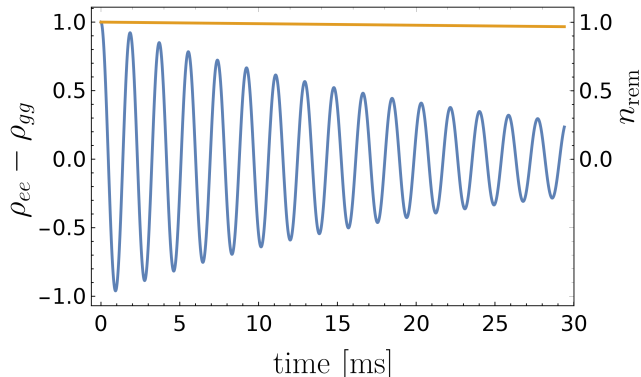


FIG. 9. The blue curve shows the time-evolution of the inversion $\rho_{ee} - \rho_{gg}$. The center of the Gaussian electron beam of waist radius $w = 50 \mu\text{m}$ is at a distance of $5w$ from the atom. We consider an average current $I_0 = 100 \mu\text{A}$ and bunching parameter $r_b = 0.5$ corresponding to a resonant current modulation at the base frequency ω_0 of amplitude $2I_0 J_1(r_b) \sim 50 \mu\text{A}$. The resulting Rabi frequency is $\Omega \approx 2\pi \times 540 \text{Hz}$. The decay of coherence is due to the assumed FWHM linewidth of the electron beam modulation of 25 Hz. We calculated (orange line) the ratio of atoms n_{rem} whose state is altered by incoherent scattering of single electrons assuming a remaining current density of 0.1% of the peak value at the position of the atoms as a conservative estimate. After 20ms, less than 1% of the atoms undergo an incoherent scattering interaction with the electrons.

We assume that the atom is in the hyperfine ground state $F=1$, $m_F=0$ and is not spatially moving on the time scale of the proposed experiment. Fig.9 plots the simulated hyperfine state response while applying an intensity modulated electron beam with a waist radius of $w = 50 \mu\text{m}$ and a current of $I = 100 \mu\text{A}$ at a distance of $d = 5w = 250 \mu\text{m}$ (beam center to atom), which is modulated on resonance with the hyperfine frequency and bunching parameter $r_b = 0.5$. We evaluated the time evolution of the atomic state based on the modified optical Bloch equations (110) in Mathematica using NDSolve. At a kinetic energy of 18 keV, a frequency of 254 MHz corresponds to λ_0 of about 30 cm. Therefore, the condition $d \ll \lambda_0$ that we introduced above is fulfilled and we can use equation (102) for the description of the expected field strength. Several Rabi oscillations of the hyperfine states are clearly visible in the plot. The source of the decay of coherence is technical noise in the electron beam source which we assumed to lead to a spectral linewidth of the beam modulation of about 25 Hz. We set $b = \delta\omega/2 = \pi \times 25 \text{Hz}$. Furthermore, for the transition under consideration, we have $\Gamma_1 = 2\Gamma_2 \ll b$ and we neglect Γ_1 and Γ_2 in the simulation. Systematic effects such as transition changes due to inelastic single electron atom interactions, which could also change the electronic state of the atoms, happen on a much longer time scale (see Fig.9, orange line). The total scattering cross section (causing ionization, elastic and inelastic scattering) for potassium atoms exposed to an 18 keV electron beam is $\sigma_{\text{tot}} \approx 1.5 \cdot 10^{-17} \text{cm}^2$, extrapolated from [36].

We now estimate the Doppler shift experienced by atoms in a normal cold atom experiment. If the velocity of the atoms Δv_a is small compared to the speed of the electron beam modulation v , the observed frequency shift of a moving atom compared to a non-moving atom can be approximated by $\Delta f = \Delta v_a f_0 / v_e$. Potassium atoms at a temperature of 40 μK move with a most probable velocity of 0.12 m/s and will experience an intensity modulated electron beam (velocity of the electron $v = c/4$) of frequency 254 MHz in the lab frame with a detuning of around 0.02 Hz, which is negligible.

12. EXAMPLE 2: NV CENTERS IN NANO DIAMONDS

In the following, we will consider Nitrogen Vacancy (NV) centers in nano-diamonds as an example of the case where nano-meter distances between an electron beam and a quantum system can be maintained. In this situation, the magnetic near field consists of distinct spikes due to the well separated electrons. Therefore, using the expected value for the magnetic field in the optical Bloch equations would not be appropriate and we simulate the effect of the magnetic field of each electron separately. In particular, we will focus on the transition between the 3A_2 ground state magnetic sublevels $m_s = 0$ and $m_s = 1$, which are split by $\omega_0 = 2.87 \text{GHz}$ [37]. The $m_s = -1$ sub-level is

well separated from the $m_s = 1$ sublevel by ~ 4 MHz [38] such that the transition from $m_s = 0$ to $m_s = 1$ can be individually addressed. We consider the z -direction as the quantization direction, with the magnetic field oriented in the x -direction. Then, we find for the transition matrix elements $T_{0,1} = g_S \mu_B B_x / \sqrt{2}$ (see section 9). This transition exhibits coherence times T_2 from $600 \mu\text{s}$ [39] up to 600 ms ([40] using a dynamical decoupling pulse sequence), which is the main decay channel for the Rabi oscillations of the NV center. We set $T_1 = 6$ ms, $T_2 = 3$ ms here following [40]. As the electron beam source, we consider a standard scanning electron microscope generating a beam waist of $w = 1$ nm, beam energy of 30 keV, a probe current of 5 nA (corresponding to ~ 10 electrons per modulation period) and a bunching parameter $r_b \approx 0.5$ ($l = 11$ cm and $\delta E_{\text{kin}}/E_{\text{kin}} = 1/20$) directed next to an NV center at a distance of $d = 5w = 5$ nm, for example embedded in a free standing nanostructure [41]. We assume that the beam is modulated by velocity modulation and bunching with a spectral modulation linewidth of $10^{-7} \omega_0 / (2\pi) \sim 300$ Hz. The result of a simulation of the expected level response is given in Fig.10. To reduce unwanted systematic effects due to electron scattering on the diamond structure [42] we need to ensure that the electron beam intensity at the position of the NV center is reduced by a factor of 10^{-7} compared to its maximum. At this intensity, which is easily fulfilled for a Gaussian beam at $5w$, on average less than one electron scatters within a radius of 1 nm next to the NV center every inverse Rabi frequency.

To produce the data for Fig.10, an array of the full number of electrons is generated. We modulate the kinetic energy of the particles and calculate the propagation over the drift distance l to obtain the current modulation. The modulation of kinetic energy is sinusoidal $E_{\text{kin}}(t) = E_{\text{kin},0} + \Delta E_{\text{kin}} \sin(\omega_0 t + \phi(\xi, t))$, where $\phi(\xi, t)$ is a random process incorporating the finite linewidth of the driving. In particular, $d\phi(\xi, t)/dt = F(\xi, t)$, where $E[F(\xi, t), F(\xi, t')] = 2b\delta(t - t')$ which implies that for each temporal interval $[a, b]$, we have

$$\text{Var}(\phi(\xi, a) - \phi(\xi, b)) = 2b|a - b|. \quad (145)$$

Based on this variance and a vanishing average, the phase noise was implemented as a random Gaussian process. Then, the optical Bloch equations in the rotating frame were solved consecutively for each interaction of an electron with NV-center over a short interaction period on the order of $d/(\gamma v)$ using the Python ODE solver `solve_ivp`. Since the beam is very dilute (only about 10 electrons per modulation period, i.e. the average distance between two electrons in the beam divided by d is on the order of 10^5), the interaction regions of two electrons will rarely overlap and the approximation of consecutive interactions is justified. Finally, the result of several runs were averaged to obtain an average over different realizations of phase noise.

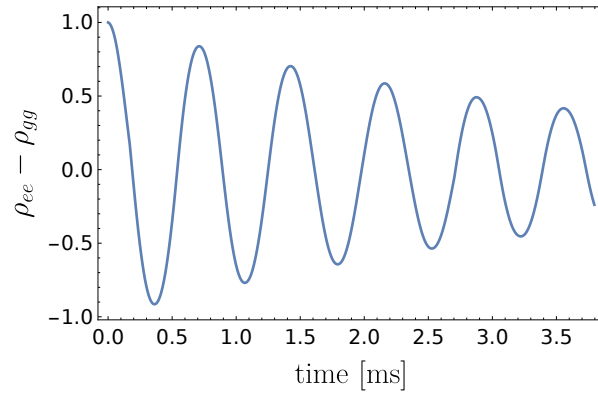


FIG. 10. Time-evolution of the inversion for the transition $m_s = 0 \rightarrow m_s = 1$ in the 3A_2 -state of an NV center at distance $d = 5$ nm from a beam of waist 1 nm, current 5 nA and bunching parameter $r_b \approx 0.5$ ($l = 11$ cm and $\delta E_{\text{kin}}/E_{\text{kin}} = 1/20$). We set $T_1 = 6$ ms, $T_2 = 3$ ms and the FWHM linewidth of the electron beam modulation $b/\pi = 300$ Hz.